Geometrically exact post-buckling and post-flutter of standing cantilevered pipe conveying fluid

Amir Mehdi Dehrouyeh-Semnani[1]

School of Mechanical Engineering, College of Engineering, University of Tehran, Tehran, Iran

Abstract

Although the nonlinear dynamics of hanging cantilevered pipes conveying fluid have been extensively scrutinized, there is limited research on the nonlinear behavior of standing ones. Hence, the objective of this study is to examine the geometrically exact nonlinear static and dynamic responses of cantilevered pipes conveying fluid in a standing position. The geometrically exact rotation-based model, combined with the shooting method and the Galerkin technique, is applied to assess the nonlinear static behavior of system and its stability characteristics. Moreover, to compute the nonlinear dynamics of system, the geometrically exact quaternion-based model, together with the Galerkin technique, is employed. It is revealed that the system may undergo buckling through either a supercritical or subcritical pitchfork bifurcation, depending on the gravity parameter, which may give rise to extremely large-amplitude responses. The system may also experience flutter instability due to a supercritical Hopf bifurcation, which brings about self-excited periodic oscillations. The generic behavior of system for a specific range of the gravity parameter is investigated across four distinct scenarios, which vary based on the gravity parameter and mass ratio. Notably, only one of these scenarios is analogous to the situation that comes to pass for the hanging case.

Keywords

Standing cantilevered pipe conveying fluid; Geometrically exact nonlinear analysis; Subcritical and supercritical pitchfork bifurcation; Supercritical Hopf bifurcation; Extremely large amplitude; Self-excited periodic oscillation.

1. Introduction

Pipes conveying fluid as a kind of fluid-solid interaction system, have drawn noteworthy research interest due to their applications in numerous engineering systems [1-6]. Pipes conveying fluid have also emerged as a model dynamical problem [7]. This model serves as a valuable framework for comprehending the dynamics of complex systems, as well as a means of exploring novel phenomena and dynamic characteristics [7]. Furthermore, cantilevered pipe conveying fluid represents one of the few instances in engineering applications of a non-conservative elastic system influenced by a follower force which is characterized by its continuous tangential alignment with the deflected axis of the slender structure [3].

[1] Email addresses: a.m.dehrouye@ut.ac.ir, a.m.dehrouye@gmail.com (A.M. Dehrouyeh-Semnani)

It is well-known that fluid-conveying pipes supported at both ends undergo buckling instability at sufficiently high flow velocities [3, 8]. The stability characteristics, along with the nonlinear static and dynamic responses of these pipes, have been extensively analyzed [3, 9-19]. According to the existing literature, the theoretical and experimental studies on the flutter instability of cantilevered pipes conveying fluid were first introduced in the papers by Bourrières [20], Benjamin [21, 22], Paidoussis and Gregory [23, 24] and Paidoussis [25]. Baja et al. [26, 27] developed a nonlinear mathematical model to analyze the bifurcation behavior of cantilevered pipes conveying fluid, reporting several intriguing features of the system. However, their nonlinear mathematical model contains some incomplete terms, which are discussed in detail in Ref. [3]. Semler et al. [28] established a third-order approximate nonlinear mathematical model for the planar motion of cantilevered pipes conveying fluid, while Wadham-Gagnon et al. [29] extended this model to three-dimensional motion. In numerous studies related to cantilevered pipes conveying fluid, the third-order approximate model or its extended versions, accounting for additional elements, imperfect support, material properties, and other factors, have been utilized to examine the nonlinear dynamics of system [30-39]. Since the third-order approximate model was derived [28] based on the assumption of inextensibility, Ghayesh et al. [40] developed a new approximate model from which the third-order approximate model can be recovered, to explore the role of extensibility in the nonlinear dynamics of cantilevered pipes conveying fluid.

Recently, the geometrically exact modeling and analysis of cantilevered pipes conveying fluid have garnered significant research interest due to the limitations of the third-order approximate model in simulating of large-amplitude responses of the system. Geometrically exact models for dynamic analysis of cantilevered pipes conveying fluid have been developed using four distinct approaches. In the first approach, a geometrically exact model within an intrinsic orthogonal framework was developed based on the Cosserat rod model [41]. The second approach proposed a geometrically exact model based on the total moment of both the fluid and the pipe [42]. The fully nonlinear differential governing equations of system were established according to the momentum balance of pipe and fluid in floating non-inertial frames. The third approach involves developing a geometrically exact model in terms of the rotation angle, utilizing Hamilton's principle from which the third-order approximate model can be recovered [43-49]. The fourth approach is associated with deriving a geometrically exact model based on quaternion formulation, in conjunction with Hamilton's principle [50]. It was indicated that the rotational-based model developed in Ref. [43] can be recovered from the newly developed model. A major difference between this model and that developed in Ref. [43] is that its governing equations are expressed in terms of integro-partial differential algebraic equations, whereas the governing equation of the model presented in Ref. [43] is an integro-partial differential equation. Comparative studies indicated that the quaternion-based model is capable of capturing the nonlinear dynamics of system while achieving a remarkable reduction in computational cost compared to the rotation-based model.

The nonlinear dynamics of standing cantilevered pipes conveying fluid have been investigated in a few studies. Li and Paidoussis [51] examined the nonlinear dynamics of such pipes using the third-order approximate model in conjunction with the Galerkin technique, employing two modes. Prior to applying Galerkin's technique, the non-linear inertia terms were substituted with equivalent terms through a perturbation procedure. This study focused on stability and double degeneracy, where subcritical pitchfork bifurcation and Hopf bifurcation occur simultaneously, as well as on the chaotic motion of the system. Wang and Ni [52] studied the stability and chaotic motions of standing cantilevered pipes conveying fluid with elastic support and motion-limiting constraints. In their mathematical model, the source of nonlinearity stemmed from the support and constraints, while a linear model was adopted for the pipe conveying fluid. Similar to the previous reference, Galerkin's technique with two modes was used for system analysis. Bou-Rabee et al. [53] investigated the stability characteristics of standing cantilevered pipes conveying fluid using a simple geometrically exact model. To construct the mathematical model, they supposed that the fluid-structure interaction induces a concentrated force and a point source of damping, which are tangent and normal to the free end, respectively. A long, thin conduit with a nozzle at its free end serves as an appropriate representation for this model. Chen et al. [54] analyzed the nonlinear behavior of standing cantilevered pipes conveying fluid based on the geometrically exact rotation-based model for a specific case (see Appendix A). It is worth noting that Farokhi et al. [55, 56] experimentally validated the geometrically exact nonlinear model for extremely large-amplitude vibrations of a standing cantilevered beam subjected to harmonic excitation. The findings indicate that when the cantilevered beam undergoes large-amplitude vibrations, the results of third-order nonlinear model are not reliable; however, the geometrically exact nonlinear model effectively captures the experimental measurements.

The review of papers related to the nonlinear analysis of cantilevered pipes conveying fluid shows that the nonlinear dynamics of standing systems have not been adequately addressed, in contrast to hanging and horizontal systems. Therefore, the focus of this paper is to explore the geometrically exact nonlinear static and dynamic behavior of standing cantilevered pipes conveying fluid. In Section 2, two distinct mathematical models utilized to acquire the geometrically exact nonlinear responses of system are explained in detail. As well, the solution strategies for determining the static, stability, and dynamic behavior of system are elucidated. In Section 3, the available results from the existing literature concerning the geometrically exact nonlinear dynamics of standing cantilevered pipes conveying fluid are employed to verify the mathematical model and solution strategy used in this paper for dynamic analysis. A convergence study on the verified results is also presented in this section. In Section 4, a geometrically exact nonlinear analysis of the generic behavior of system is conducted. First, the stability of undeformed configuration of system without flow velocity due to gravity, along with its stable positions, is examined. Subsequently, the influence of flow velocity, in conjunction with the gravity parameter, on new static responses and their stability is analyzed. The role of flow velocity, along with the gravity parameter and mass ratio, in dynamic instability and corresponding motion characteristics is also investigated. A generic behavior for four distinct scenarios is discussed in detail.

Additionally, the impact of initial conditions on the final response of system is explored. A comparative study with the results of the third-order nonlinear model is also conducted. Finally, a summary of the findings is presented in Section 5.

2. On mathematical models and solution strategies

A schematic representation of a cantilevered pipe in a standing position, which conveys fluid, is illustrated in Figure 1. The system under investigation consists of a pipe of length L, cross-sectional area A, flexural rigidity EI, mass per unit length m, conveying a fluid of mass per unit length M with flow velocity $\overline{U}$.

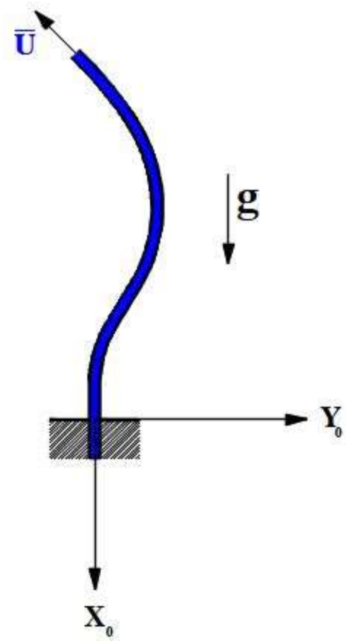

Figure 1: Schematic representation of a standing cantilevered pipe conveying fluid

To assess the geometrically exact static responses of system, the geometrically exact rotation-based model (GERM) is used. The reason for choosing this model is that it effectively captures the static responses of system in conjunction with the shooting scheme. However, to determine stability characteristics of the nonlinear static responses, Galerkin's technique is utilized. For the dynamic analysis, the geometrically exact quaternion-based model (GEQM), along with the Galerkin technique, is implemented. The advantage of this model over the former is its lower computational cost. It should be pointed out that the mathematical models for hanging and standing cantilevered pipes conveying fluid are identical, except for the gravity parameter. In the case of the hanging pipe, the gravity parameter is positive, while it is negative for the standing pipe. Therefore, the geometrically exact mathematical models developed in previous studies for hanging cantilevered pipes conveying fluid can also be applied to the standing pipes. Finally, it should be mentioned that to let the analysis of not just one specific system but a generalized system, despite of size and material properties, dimensionless quantities are utilized to examine the nonlinear behavior of system [3].

2.1. Static and stability analyses via GERM

The dimensionless form of the geometrically exact equation of motion and the corresponding boundary conditions for a cantilevered pipe conveying fluid in terms of rotation angle, θ, were established as follows [43, 44, 54]

$$\begin{aligned}
&\theta'' + (1-s)\gamma\sin(\theta) - \alpha\dot{\theta}'' + U^2\sin(\theta(1)-\theta) \\
&+\cos(\theta)\int_1^s\left[\int_0^{\hat{s}}\left((\dot{\theta})^2\sin(\theta)-\ddot{\theta}\cos(\theta)\right)d\hat{\hat{s}}\right]d\hat{s} \\
&-\sin(\theta)\int_1^s\left[\int_0^{\hat{s}}\left((\dot{\theta})^2\cos(\theta)+\ddot{\theta}\sin(\theta)\right)d\hat{\hat{s}}\right]d\hat{s} \\
&-2U\sqrt{\beta}\left(\sin(\theta)\int_1^s\dot{\theta}\sin(\theta)\,d\hat{s}+\cos(\theta)\int_1^s\dot{\theta}\cos(\theta)\,d\hat{s}\right)=0,
\end{aligned} \tag{1}$$

$$\theta(0)=0,\ \ \theta'(1)=0, \tag{2}$$

where the dimensionless quantities are

$$s=\frac{s^*}{L},\ \ (\tau,\alpha)=\sqrt{\frac{EI}{(M+m)L^4}}\left(t,\alpha^*\right),\ \mathrm{U}=\left(\frac{M}{EI}\right)^{1/2}\bar{\mathrm{U}},\ \beta=\frac{M}{M+m},\ \ \gamma=\frac{M+m}{EI}gL^3, \tag{3}$$

in which s is dimensionless distance along the pipe from the clamped end, ζ and η, respectively, are dimensionless axial and transverse displacements, τ is dimensionless time, α is dimensionless damping coefficient, U is dimensionless flow velocity, β is mass parameter, and γ is gravity parameter. Moreover, the prime and dot symbols denote derivatives with respect to s and τ, respectively. The dimensionless axial and transverse displacements, respectively, can be obtained by [43]

$$\zeta=\frac{u}{L}=\int_0^s\cos(\theta(\hat{s}))\,d\hat{s}-1,\ \ \eta=\frac{v}{L}=\int_0^s\sin(\theta(\hat{s}))\,d\hat{s}. \tag{4}$$

The geometrically exact rotation-based static model can be obtained by eliminating the time-dependent terms from Eq. (1) [54].

$$\theta_s''+(1-s)\gamma\sin(\theta_s)+U^2\sin(\theta_s(1)-\theta_s)=0, \tag{5}$$

in which θ_s stands for static rotation angle. Similar to Ref. [57], the shooting scheme is used to evaluate the geometrically exact responses of system based on the static equation given in Eq. (5). To determine their stability, the linearized dynamic model around the static responses is employed. Substituting $\theta+\theta_s$ instead of θ in Eq. (1), incorporating Eq. (5), and neglecting the nonlinear terms in the resulting equation, one can acquire the following linear dynamic equation [54].

$$\theta'' + (1-s)\gamma\sin(\theta^s)\theta - \alpha\dot{\theta}'' + U^2(\theta(1)-\theta)\cos(\theta^s(1)-\theta^s)$$
$$+\cos(\theta^s)\int_1^s\left[\int_0^{\hat{s}} -\ddot{\theta}\cos(\theta^s)ds'\right]d\overline{s} - \sin(\theta^s)\int_1^s\left[\int_0^{\hat{s}}\ddot{\theta}\sin(\theta^s)d\hat{s}\right]d\hat{s} \tag{6}$$
$$-2U\sqrt{\beta}\left(\sin(\theta^s)\int_1^s\dot{\theta}\sin(\theta^s)d\hat{s} + \cos(\theta^s)\int_1^s\dot{\theta}\cos(\theta^s)d\hat{s}\right) = 0,$$

In view of Galerkin's technique, the rotation angle is approximated as follows

$$\theta = \sum_{n=1}^{N}\varphi_n p_n, \tag{7}$$

in which N, φ_n and p_n stand for number of approximate functions, nth approximate function, and nth generalized coordinate, respectively. Similar to Ref. [54], $\varphi_n = sin((2n-1)\pi s/2)$. It should be mentioned that to calculate the stability characteristics of system around its undeformed configuration, it is enough to set $\theta_s = 0$ in Eq. (6).

2.2. Dynamic analysis via GEQM

The geometrically exact mathematical model of cantilevered pipe conveying fluid in the quaternion system was derived in Ref. [50]. The quaternion elements e_0 and e_3 can be written in terms of the rotation angle as follows [50]: $e_0 = cos(\theta/2)$ and $e_3 = sin(\theta/2)$, along with the following constraint: $\Phi = e_0^2 + e_3^2 = 1$. The resulting dimensionless form of this mathematical model is [50] as follows

$$4\left(e_0{}''e_3^2 - e_0e_3e_3{}'' - 2e_0(e_3')^2 + 2e_0'e_3e_3'\right) + \gamma(2e_0)(1-s)$$
$$+\left[2e_0\int_1^s\int_0^{\hat{s}}2\left(e_0\ddot{e}_0 + (\dot{e}_0)^2 - e_3\ddot{e}_3 - (\dot{e}_3)^2\right)d\hat{s}d\hat{s}\right] + \left[2e_3\int_1^s\int_0^{\hat{s}}2(e_0\ddot{e}_3 + 2\dot{e}_0\dot{e}_3 + e_3\ddot{e}_0)d\hat{s}d\hat{s}\right]$$
$$+2U\sqrt{\beta}\left(\left[2e_0\int_1^s 2(e_0\dot{e}_0 - e_3\dot{e}_3)d\hat{s}\right] + \left[2e_3\int_1^s 2(e_3\dot{e}_0 + \dot{e}_3e_0)d\hat{s}\right]\right) \tag{8}$$
$$-U^2\left[2e_0\left(e_0^2(1) - e_3^2(1)\right) + 2e_3\left(2e_0(1)e_3(1)\right)\right] - \alpha\left[-8\left(e_3'e_3\dot{e}_0' + e_3'e_0'\dot{e}_3 - e_3'e_3'\dot{e}_0 - e_3'e_0\dot{e}_3'\right) -\right.$$
$$\left.4\left(e_3e_3'\dot{e}_0' + e_3e_3\dot{e}_0'' + e_3e_0'\dot{e}_3' + e_3e_0''\dot{e}_3 - e_3e_3''\dot{e}_0 - e_3e_3'\dot{e}_0' - e_3e_0\dot{e}_3'' - e_3e_0'\dot{e}_3'\right)\right] - 2e_0\lambda = 0,$$

$$4\left(e_0^2e_3{}'' - e_0e_0{}''e_3 - 2(e_0')^2e_3 + 2e_0e_0'e_3'\right) - \gamma(2e_3)(1-s)$$
$$-\left[2e_3\int_1^s\int_0^{\hat{s}}2\left(e_0\ddot{e}_0 + (\dot{e}_0)^2 - e_3\ddot{e}_3 - (\dot{e}_3)^2\right)d\hat{s}d\hat{s}\right] + \left[2e_0\int_1^s\int_0^{\hat{s}}2(e_0\ddot{e}_3 + 2\dot{e}_0\dot{e}_3 + e_3\ddot{e}_0)d\hat{s}d\hat{s}\right]$$
$$-2U\sqrt{\beta}\left(\left[2e_3\int_1^s 2(e_0\dot{e}_0 - e_3\dot{e}_3)d\hat{s}\right] - \left[2e_0\int_1^s 2(e_3\dot{e}_0 + \dot{e}_3e_0)d\hat{s}\right]\right) \tag{9}$$
$$-U^2\left[-2e_3\left(e_0^2(1) - e_3^2(1)\right) + 2e_0\left(2e_0(1)e_3(1)\right)\right] - \alpha\left[8\left(e_0'e_3\dot{e}_0' + e_0'e_0'\dot{e}_3 - e_0'e_3'\dot{e}_0 - e_0'e_0\dot{e}_3'\right) +\right.$$
$$\left.4\left(e_0e_3'\dot{e}_0' + e_0e_3\dot{e}_0'' + e_0e_0'\dot{e}_3' + e_0e_0''\dot{e}_3 - e_0e_3''\dot{e}_3 - e_0e_3'\dot{e}_0' - e_0e_0\dot{e}_3'' - e_0e_0'\dot{e}_3'\right)\right] - 2\lambda e_3 = 0,$$
$$e_0^2 + e_0^3 = 1, \tag{10}$$

$$e_0(0)=1,\ e_3(0)=0,\ e_0'(1)=0,\ e_3'(1)=0, \tag{11}$$

in which λ is dimensionless Lagrangian multiplier function. The dimensionless axial and transverse displacements in terms of the quaternion elements, respectively, can be written [50]

$$\zeta=\int_0^s\left(e_0^2-e_3^2\right)d\hat{s}-1,\ \ \eta=\int_0^s 2e_0e_3\ d\hat{s}. \tag{12}$$

The mathematical model of system in terms of the rotation angle is an integro-partial differential equation (Eq. (1)), but it is integro-partial differential algebraic equations in terms of the quaternion elements (Eqs. (8)-(9)). In Ref. [50], it was proved that Eqs. (1)-(2) can be recovered from Eqs. (8)-(11). Furthermore, it was discussed that the quaternion-based model significantly reduces computational costs compared to the rotation-based model.

In view of Galerkin's technique, the quaternion elements and the dimensionless Lagrangian multiplier function are approximated as follows

$$e_0=1+\sum_{n=1}^{N_{e_0}}\phi_n p_n,\ e_3=\sum_{n=1}^{N_{e_3}}\psi_n q_n,\ \lambda=\sum_{n=1}^{N_\lambda}\chi_n r_n \tag{13}$$

where N_{e_0}, N_{e_3}, and N_λ are number of approximate functions for e_0, e_3, and λ, respectively; ϕ_n, ψ_n, and χ_n are nth approximate function for e_0, e_3, and λ, respectively; p_n, q_n, and r_n are nth generalized coordinate of e_0, e_3, and λ, respectively. Similar to Ref. [50], $N_{e_0}=N_{e_3}=N_\lambda=N$, $\phi_n=\psi_n=sin((2n-1)\pi s/2)$ and $\chi_n=\ sin(n\pi\,(s+0.5)/4)$.

Similar to Ref. [50], to solve the resulting ordinary differential algebraic equations, the ode15s solver in MATLAB software is utilized. To reduce the index of resulting equations from three to one, Eq. (10) is replaced with the following equation [50]

$$\dot{e}_0^2+\dot{e}_3^2+e_0\ddot{e}_0+e_3\ddot{e}_3=0. \tag{14}$$

which is the second derivative of Eq. (10) with respect to τ.

3. Verification study

In Ref. [50], the quaternion-based model was utilized to verify the geometrically exact nonlinear behavior of hanging cantilevered pipe conveying fluid. Therefore, in this section, this model is verified for the standing one. Chen et al. [54] investigated the nonlinear responses of a standing pipe conveying fluid when $\beta=0.142$, $\gamma=-18.9$, and $\alpha=0.005$ via the geometrically exact rotation-based model with $N=4$. To verify the results reported in the aforementioned reference, the geometrically exact nonlinear responses of quaternion-based model with $N=4$ and 5 are calculated. Comparative studies are presented in Appendix A. The comparative studies presented in Figures A1-A3 demonstrate that the results of quaternion-based model with $N=4$ are in good agreement with those obtained by Chen et al. [54] using the rotation-based model. Additionally, the plots illustrated in these figures suggest that the quaternion-based model with $N=5$ can more accurately describe the geometrically exact nonlinear dynamics of system.

The critical flow velocities associated with the buckling and flutter instabilities, as well as the natural frequencies corresponding to the flutter instability reported by Paidoussis [25] based on the experiments, are also employed to verify the model utilized in the current study. Paidoussis' experiments on the standing cantilevered pipe conveying fluid were conducted for a system with a very small mass ratio $\beta = 1.1 \times 10^{-3}$ in which air was considered as the conveyed fluid. To theoretically simulate the pipe damping, Paidoussis utilized a hysteretic damping model in which the damping is dependent on the frequency of motion. In this study, to model the pipe damping based on the Kelvin–Voigt viscoelastic model, with the damping coefficient set to $\alpha = 0.004$. The experimental results obtained by Paidoussis [25] and the theoretical results based on the model employed in this study are presented in Figure A4 of Appendix A. Comparing the results illustrates that agreement between the experimental measurements and the theoretical results is quite good.

4. Nonlinear geometrically exact analysis

For a hanging pipe with $U = 0,$ the undeformed configuration of system is stable. However, for a corresponding standing one, the stability of undeformed configuration is dependent on the gravity parameter. The geometrically exact nonlinear static responses and their stability characteristics for the standing pipes with $-100 \le \gamma \le 0$ are plotted in Figure 2. The plots show that the undeformed configuration of system is stable when the gravity parameter is sufficiently large. However, the undeformed configuration of system becomes unstable, and the system undergoes buckling instability at a critical value of the gravity parameter $\gamma^{cr} = -7.83$. In other words, the system buckles due to its own weight (self-buckling). The plots indicate that the system undergoes extremely large deformation when the gravity parameter is sufficiently low. It should be stressed that the simple model proposed by Bou-Rabee et al. [53] is capable of capturing the geometrically exact static behavior of system. It is due to the fact that simplifications in their model do not affect the static instability of system. The results plotted in Figure 2a were presented in their work for $-60 \le \gamma \le 0$ based on a dynamic analysis. There is a good agreement between the current findings and those reported in the aforementioned reference regarding the tip rotation angle.

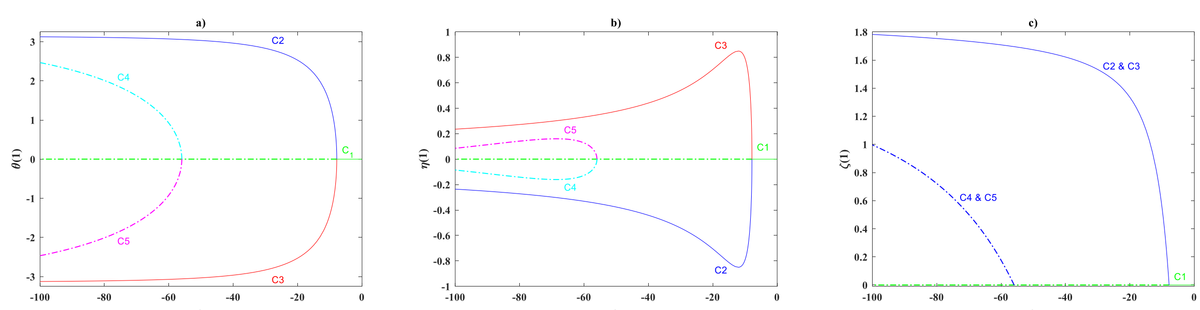

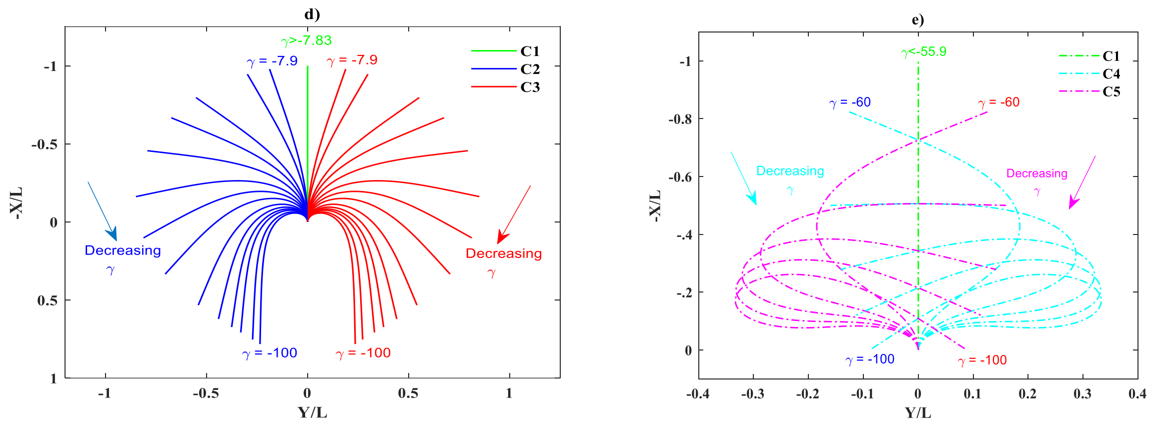

Figure 2: Evolution of the pipe shapes when $U = 0$; a) tip rotation, b) tip transverse displacement, c) tip axial displacement, d) stable shapes, e) unstable shapes.

The influence of flow velocity, U, on the static instability of system is depicted in Figure 3. The results illustrate that the system experiences a supercritical pitchfork bifurcation (buckling) when $-14 \leq \gamma < -7.83$. In other words, within this range of gravity parameter, the undeformed configuration of system becomes stable at a critical flow velocity, U_{super}. Besides, U_{super} increases as the gravity parameter is decreased. The results also indicate that the system undergoes a subcritical pitchfork bifurcation (buckling) when $\gamma < -14$. The lower subcritical velocity, U_{sub}^{low}, initially exhibits an ascending trend, followed by a descending trend as the gravity parameter is reduced. Since U_{sub}^{low} becomes zero at $\gamma = -55.9$, the lower subcritical velocity is nonexistent for the system when $\gamma < -55.9$. Additionally, the upper subcritical velocity, U_{sub}^{up}, exhibits an increasing trend as the gravity parameter decreases. It should be pointed out that both supercritical flow velocity and lower subcritical flow velocity can be determined through the stability analysis of a linear model around the undeformed configuration, when $\theta_s = 0$ in Eq. (6). The findings of this study align well with those reported by Paidoussis [3, 25] based on linear analysis.

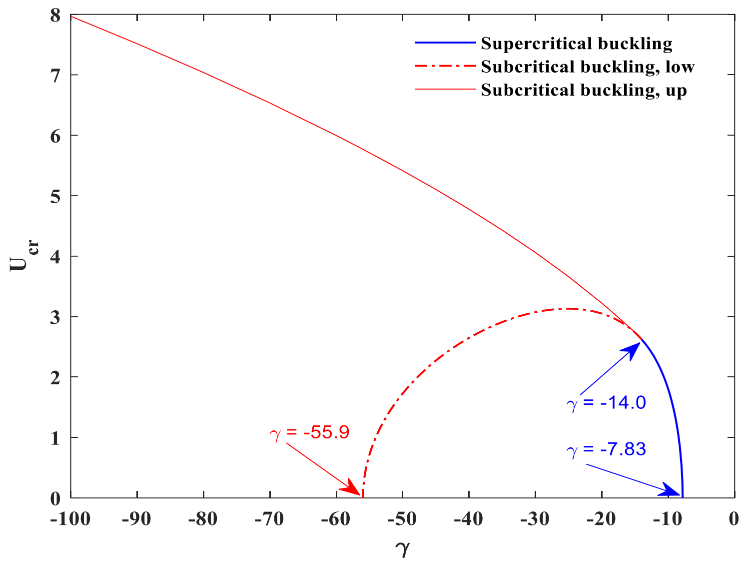

Figure 3: Locus of the critical flow velocities for the supercritical and subcritical buckling.

The geometrically exact post-buckling behavior of standing pipes conveying fluid is shown in Figures 4-6 for the tip rotation angle, and axial and transverse displacements, respectively. Figures 4a, 5a, and 6a pertain to the non-trivial post-supercritical buckling responses of system. As indicated by the results presented in these figures, when the flow velocity, U, is increased, the system undergoes reduced deformation, and at a critical flow velocity, U_{super}, the undeformed configuration of system becomes its stable position. It should be pointed out that for supercritical buckling, the undeformed configuration (the trivial solution) is unstable when $U < U_{super}$; however, the stability behavior of system for $U > U_{super}$ depends on the mass parameter, β, and the damping coefficient, α. The other plots in Figures 4-6 are associated with the non-trivial post-subcritical buckling responses of system. Similar to supercritical buckling, the system experiences reduced deformation when the flow velocity is increased; however, the trend ceases at a critical flow velocity, U_{sub}^{up}, at which the system remains in a state of deformation. The results indicate that the difference in the deformation of system between $U = 0$ and U_{sub}^{up} diminishes when the gravity parameter, γ, is lessened. It should be stressed that the undeformed configuration of system (the trivial solution) is unstable when $U \leq U_{sub}^{low}$. The stability of the trivial solution for $U > U_{sub}^{low}$ relies on β and α. It can be concluded that when $U_{sub}^{up} \leq U < U_{sub}^{low}$, the undeformed configuration of system may be stable, resulting in three distinct stable positions.

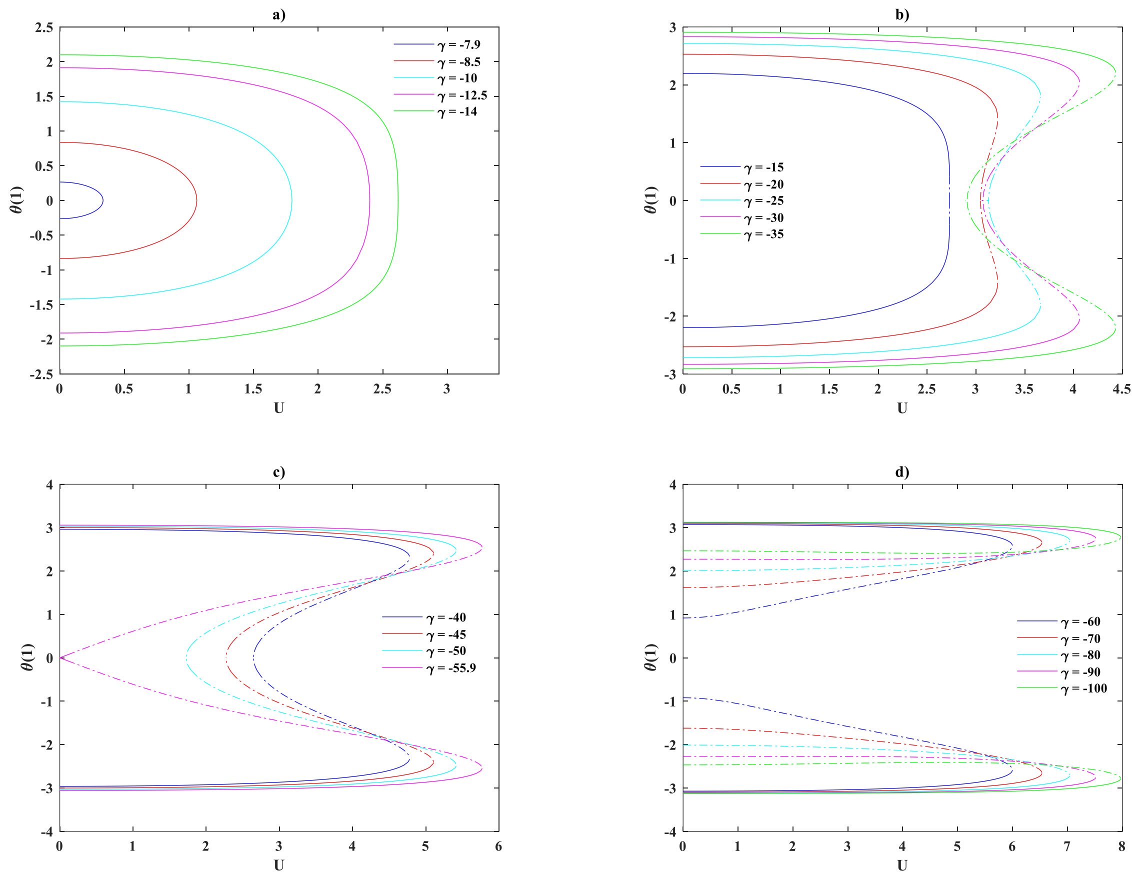

Figure 4: Stable (solid line) and unstable (dash-dot line) non-trivial solutions for the tip rotation of pipe in the post-buckling region.

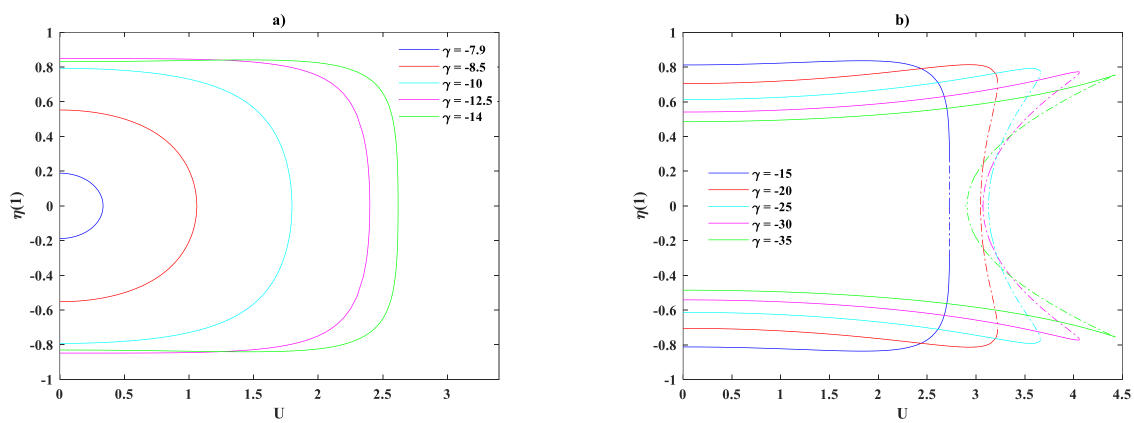

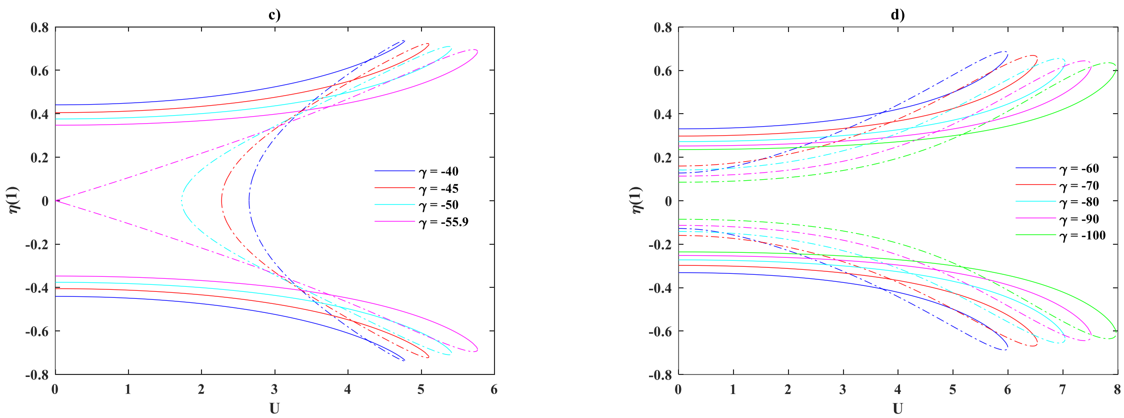

Figure 5: Stable (solid line) and unstable (dash-dot line) non-trivial solutions for the tip transverse displacement of pipe in the post-buckling region corresponding to Figure 4.

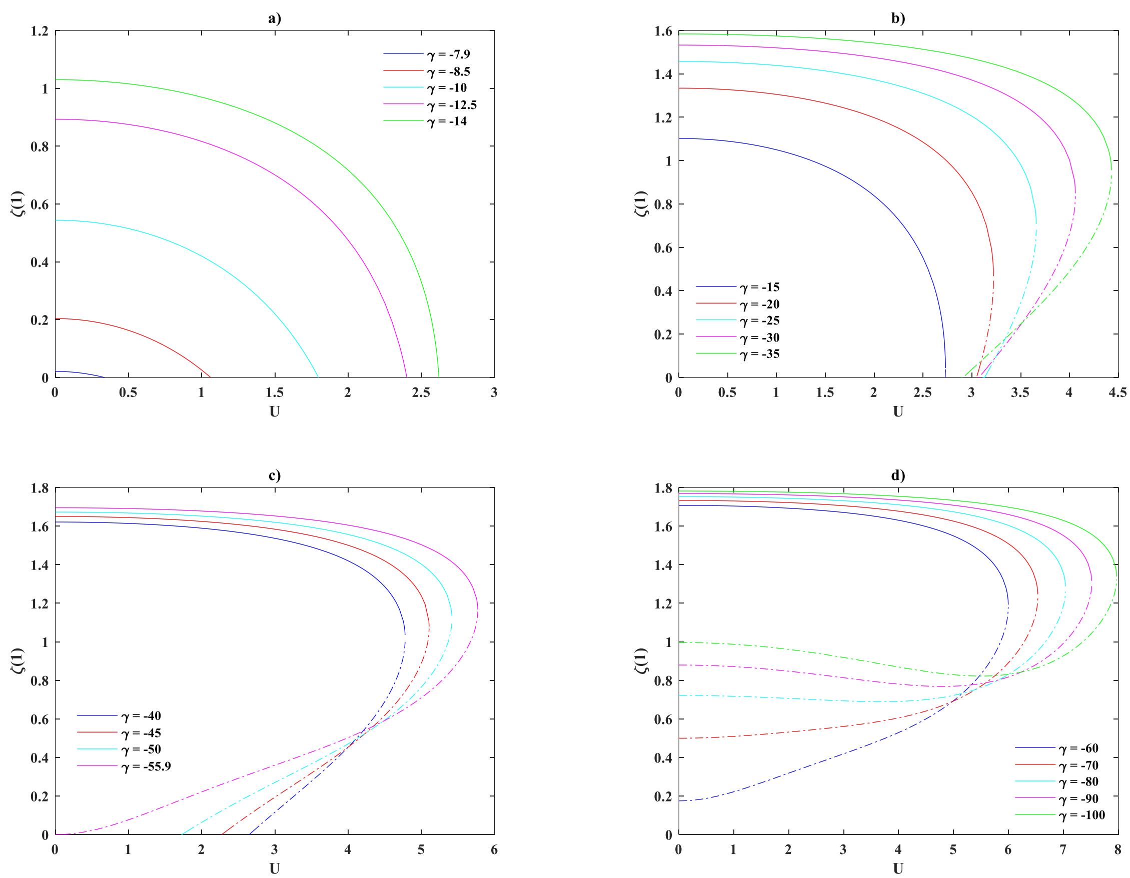

Figure 6: Stable (solid line) and unstable (dash-dot line) non-trivial solutions for the tip axial displacement of pipe in the post-buckling region corresponding to Figure 4.

Prior to commencing dynamic analysis, it is important to note that in all the dynamic assessments, the damping coefficient, α, is set to 0.005, consistent with Ref. [54]. Additionally, the whole dynamic responses are obtained using $N = 5$ in the Galerkin technique.

In the case of a hanging cantilevered pipe conveying fluid, the undeformed configuration of system is stable but becomes unstable at a critical flow velocity due to a flutter instability; specifically, the system experiences a supercritical Hopf bifurcation. As illustrated in Figure 7, a similar scenario occurs for a standing cantilevered pipe conveying fluid when the gravity parameter is sufficiently large, specifically when $\gamma < -7.83$. In the case of supercritical buckling, specifically when $-14 \leq \gamma < -7.83$, the system restabilizes at U_{super}. Subsequently, the system loses its stability at a critical flow velocity, U^f, due to a supercritical Hopf bifurcation. This flutter critical flow velocity is influenced by the mass ratio, β, the gravity parameter, γ, and the damping coefficient, α. In other words, for $-14 \leq \gamma < -7.83$, the undeformed configuration of system is stable when $U_{super} < U < U^f$. In the case of subcritical buckling i.e., $\gamma < -14$, different scenarios may take place, depending on the gravity parameter and the mass ratio. For example, when $\gamma = -20$, the undeformed configuration of system becomes stable at U_{sub}^{low} and remains stable until U^f. Since $U^f > U_{sub}^{up}$, the undeformed configuration of system is stable for $U_{sub}^{low} < U \leq U_{sub}^{up}$, exhibits three different stable positions within this range. For another example, when $\gamma = -30$ and $\beta = 0.17$ or 0.25, $U^f < U_{sub}^{up}$, the system exhibits three different stable positions for $U_{sub}^{low} < U < U^f$. Additionally, the system may undergo either post-supercritical buckling or post-flutter for $U^f < U < U_{sub}^{up}$. For $\gamma = -30$ and $\beta = 0.37$ or 0.45, the system experiences a scenario similar to that which occurs for $\gamma = -20$.

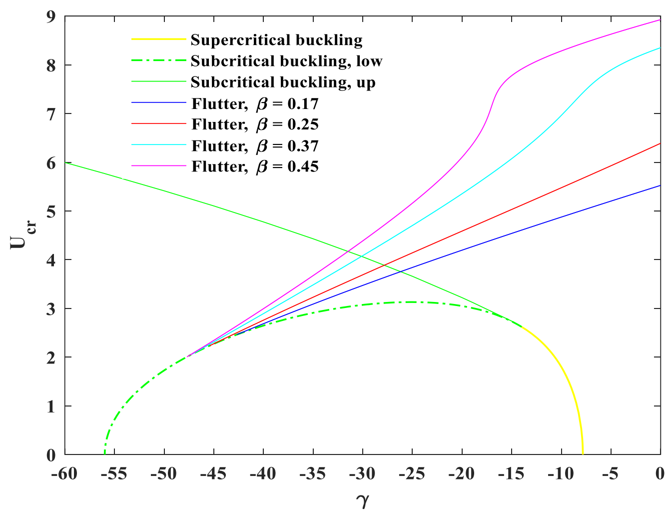

Figure 7: Locus of the critical flow velocities for the buckling and flutter instabilities.

In what comes next, four distinct scenarios regarding the generic behavior of standing cantilevered pipes conveying fluid are explored. These four scenarios are related to $\gamma = -5, -10, -20,$ and -30, along with $\beta = 0.17, 0.25, 0.37,$ and 0.45. Since the mass parameter, β, plays no role in the generic behavior of the first three scenarios, they are analyzed concurrently to more effectively illustrate evolution of the generic behavior of system when the gravity parameter, γ, is decreased. However, the impact of the mass parameter on the quantitative responses of system is comprehensively investigated. The last scenario examines the influences of both the gravity and mass parameters on the qualitative behavior of system.

The generic behavior of system with $\beta = 0.17$, and γ values of $-5, -10$, and -20, along with the range of $0 \leq U \leq 10$ is displayed in Figures 8-10. As shown in these plots in these figures, the system exhibits three distinct scenarios that depend on the gravity parameter, γ. In the first scenario involving $\gamma = -5$, the undeformed configuration of system is stable; however, it becomes unstable due to a flutter instability at a critical flow velocity $U^f = 5.2006$. For flow velocities exceeding the critical threshold, the system undergoes a supercritical Hopf bifurcation. In the second scenario, where $\gamma = -10$, the undeformed configuration of system is unstable, and the system exhibits two symmetric stable positions associated with supercritical buckling. At a critical flow velocity $U_{super} = 1.7969$, two stable positions vanish, and the undeformed configuration of system becomes stable. Afterward, the undeformed configuration of system loses its stability at a critical flow velocity $U^f = 4.8732$ at which point the system undergoes flutter instability due to a supercritical Hopf bifurcation. In the third scenario with $\gamma = -20$, the system exhibits two symmetric stable positions due to subcritical buckling when $U < U_{sub}^{up} = 3.2220$. The undeformed configuration of system is unstable until $U \leq U_{sub}^{low} = 3.0474$, at which point it becomes stable. Consequently, the system exhibits three stable positions and two symmetric unstable positions when $3.0474 < U < 3.2220$. Afterward, both the symmetric stable and unstable positions disappear and the undeformed configuration becomes unstable once more due to the occurrence of a supercritical Hopf bifurcation at $U^f = 4.1952$. It is worth noting that the plots in Figure 8 indicate that, for all three cases, the tip rotation angle of system increases when the flow velocity is raised.

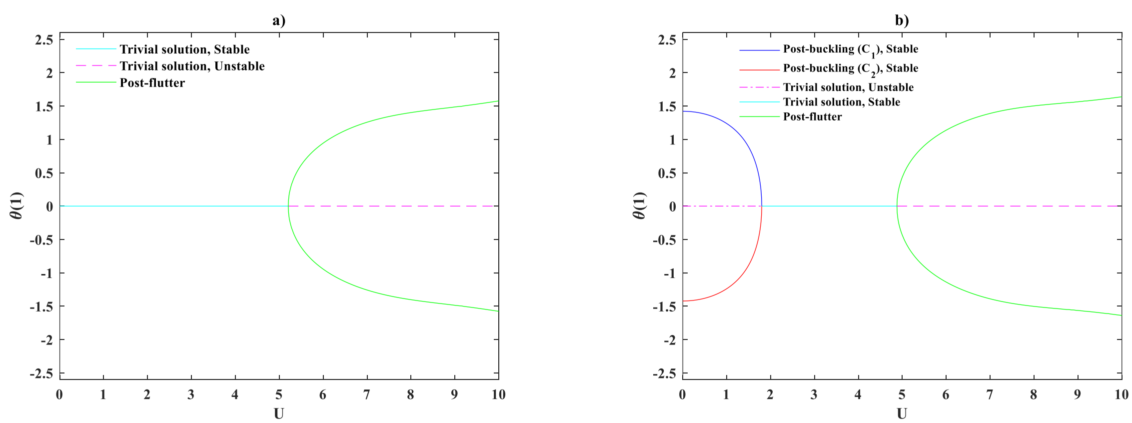

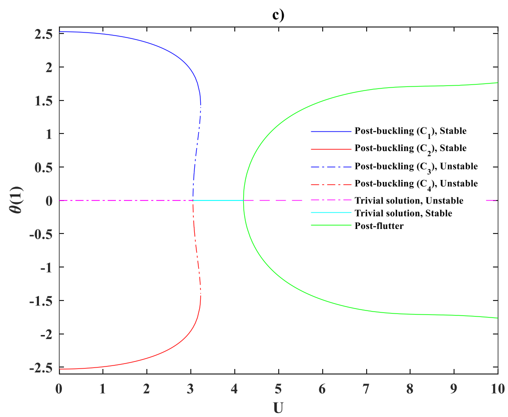

Figure 8: The tip rotation angle of pipe when $\beta = 0.17$; a) $\gamma = -5$, b) $\gamma = -10$, c) $\gamma = -20$.

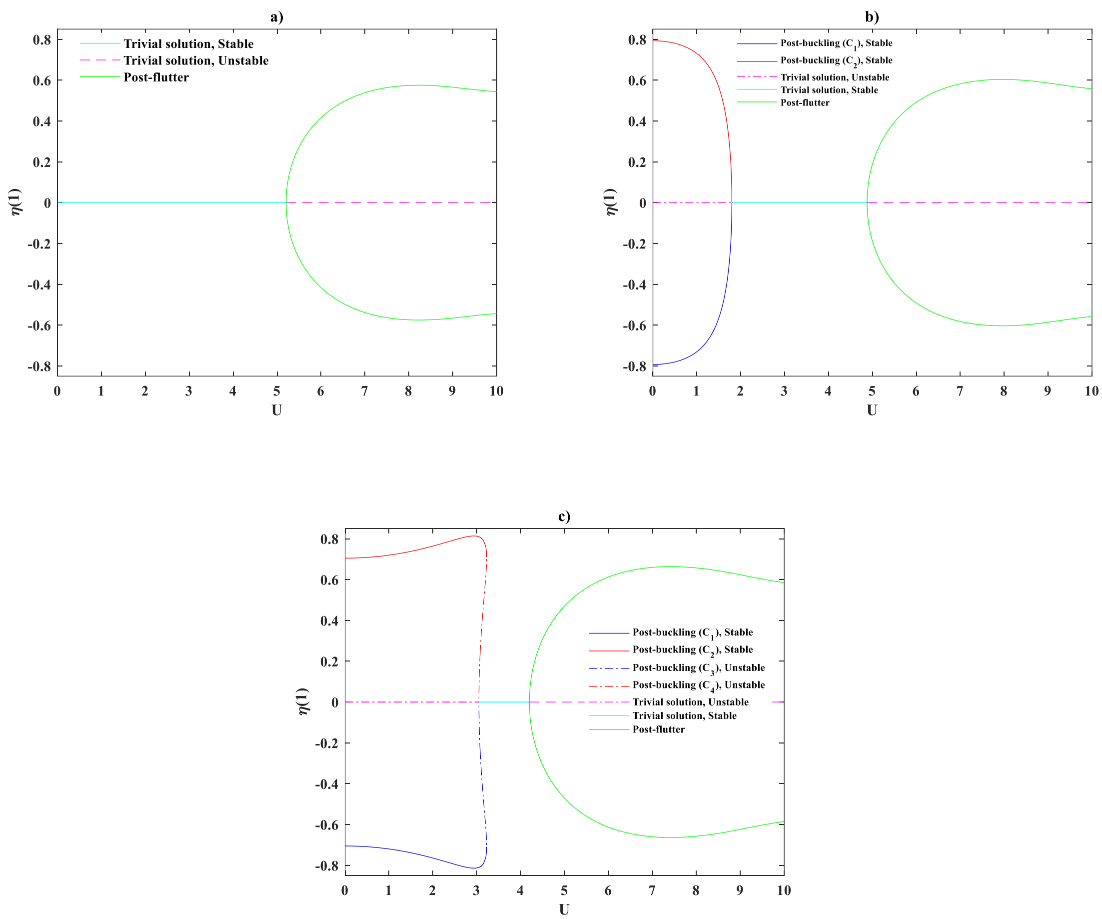

Figure 9: The tip transverse displacement of pipe corresponding to Figure 8; a) $\gamma = -5$, b) $\gamma = -10$; c) $\gamma = -20$.

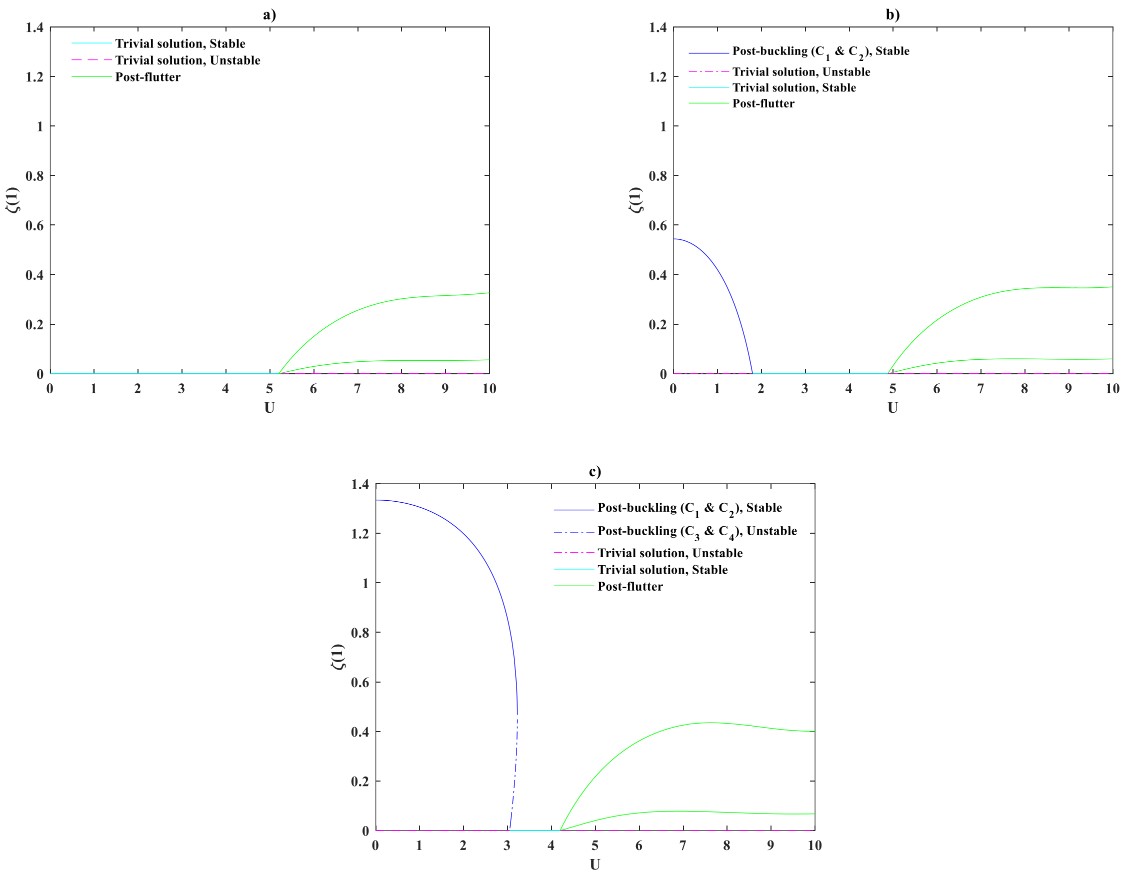

Figure 10: The tip axial displacement of pipe corresponding to Figure 8; a) $\gamma = -5$, b) $\gamma = -10$; c) $\gamma = -20$.

The two symmetric stable positions of system with $\gamma = -10$ and -20, corresponding to the supercritical and subcritical bucklings, are illustrated in Figure 11. It can be observed that when the flow velocity gradually increases, the system with $\gamma = -10$ settles down into its undeformed configuration at $U = 1.7969$. In contrast, for $\gamma = -20$, a different scenario arises due to a gradual increase in flow velocity. The system remains deformed until $U = 3.2220$. However, a slight increase in the critical flow velocity results in a sudden transition, causing the system to settle down into its undeformed configuration (see Figure 8c).

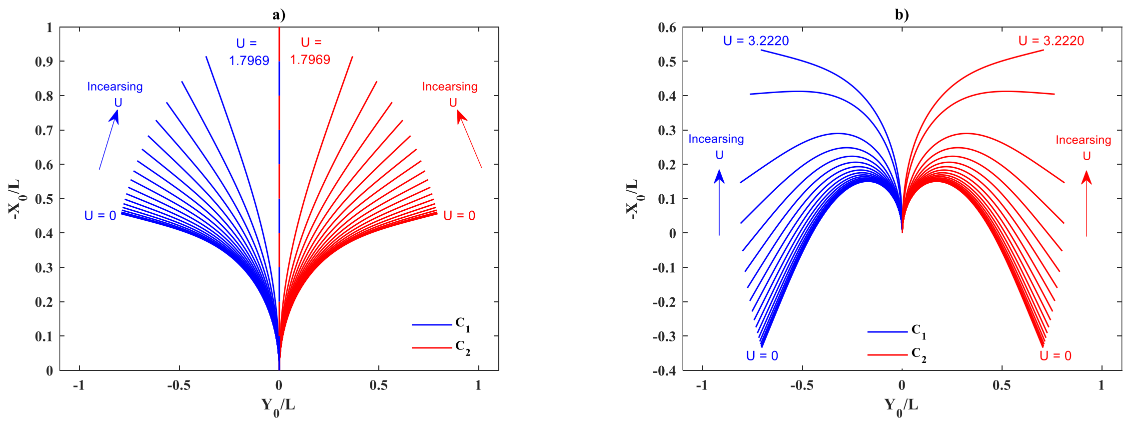

Figure 11: Evolution of the stable buckled shapes of pipe corresponding to the non-trivial solutions when $\beta = 0.17$; a) $\gamma = -10$ (supercritical buckling), b) $\gamma = -20$ (subcritical buckling).

The evolution of pipe shapes in the post-flutter region for the third case is exhibited in Figure 12. Additionally, the corresponding phase planes of system for the tip rotation angle, tip axial, and transverse displacements are displayed in Figure 13.

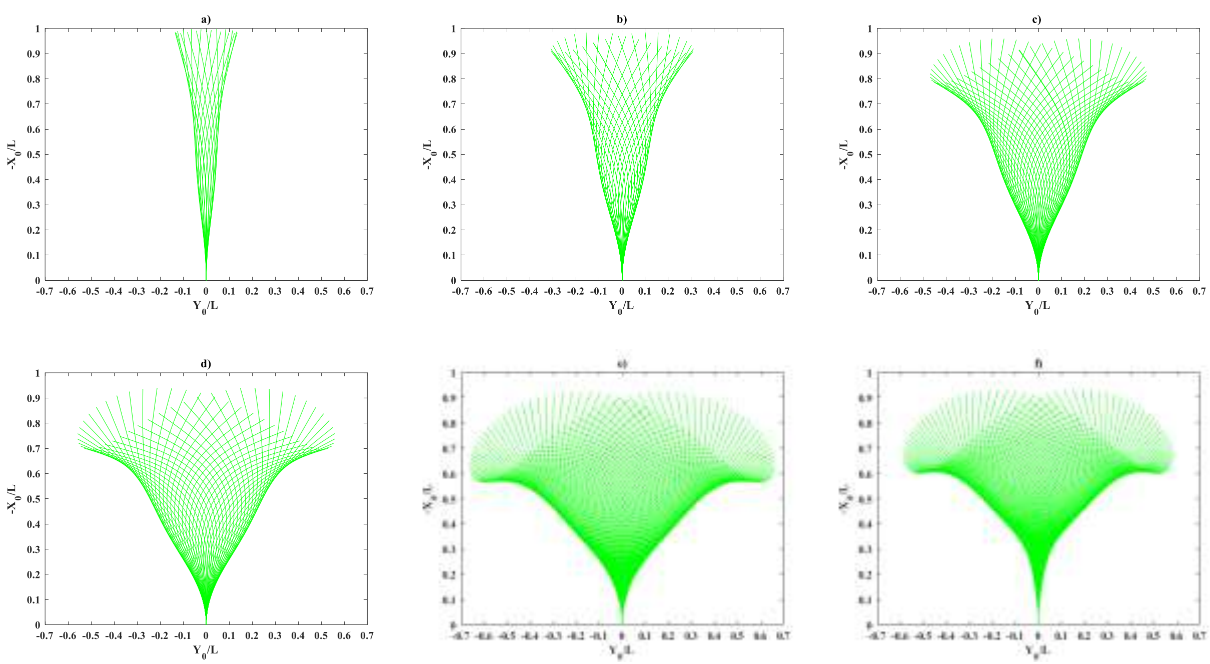

Figure 12: Shapes of the oscillating pipe in the post-flutter region when $\beta = 0.17$, $\gamma = -20$; a) $U = 4.25$, b) $U = 4.5$, c) $U = 5$, d) $U = 5.5$, e) $U = 7.5$, f) $U = 10$.

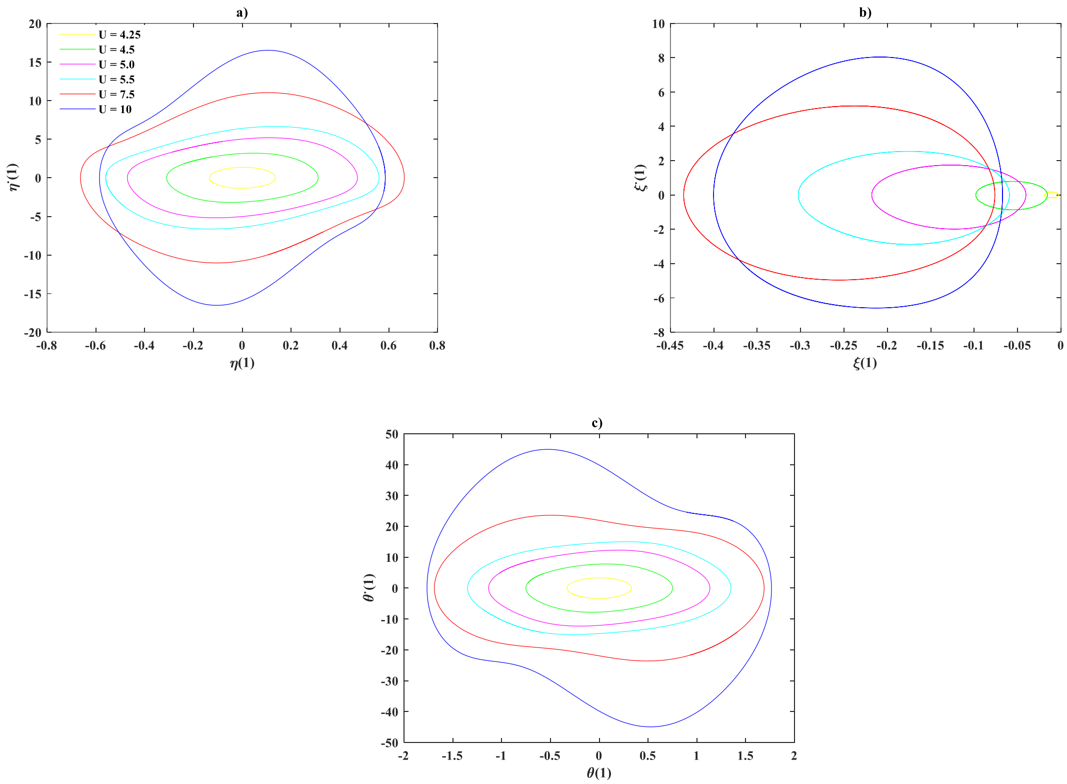

Figure 13: Phase planes of the oscillating pipe in the post-flutter region corresponding to Figure 12.

In view of Figure 7, the scenarios depicted for the system with $\beta = 0.17$ in Figures 8-10 can similarly be represented for the systems with $\beta = 0.25, 37,$ and 0.45, with the exception of the critical flow velocity associated with flutter instability. Consequently, for the aforementioned cases, only their post-flutter responses are analyzed in Figures 14-17. To facilitate a more effective comparison of the results, the post-flutter behavior of system with $\beta = 0.17$ are also included in these figures.

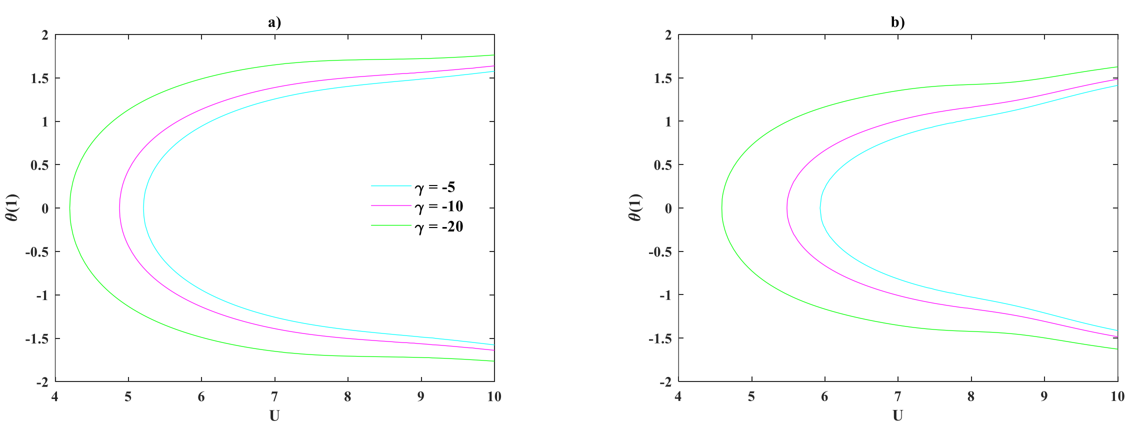

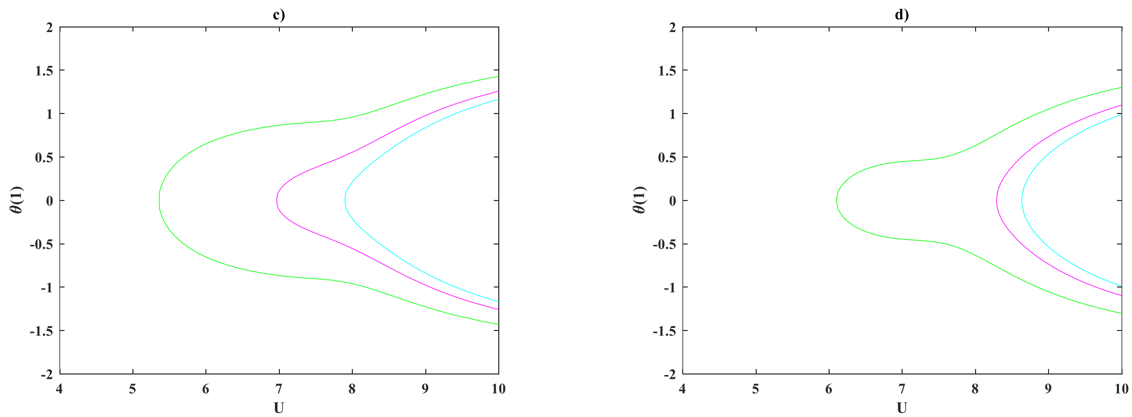

Figure 14: The tip rotation of pipe in the post-flutter region; a) $\beta = 0.17$, b) $\beta = 0.25$, c) $\beta = 0.37$, d) $\beta = 0.45$.

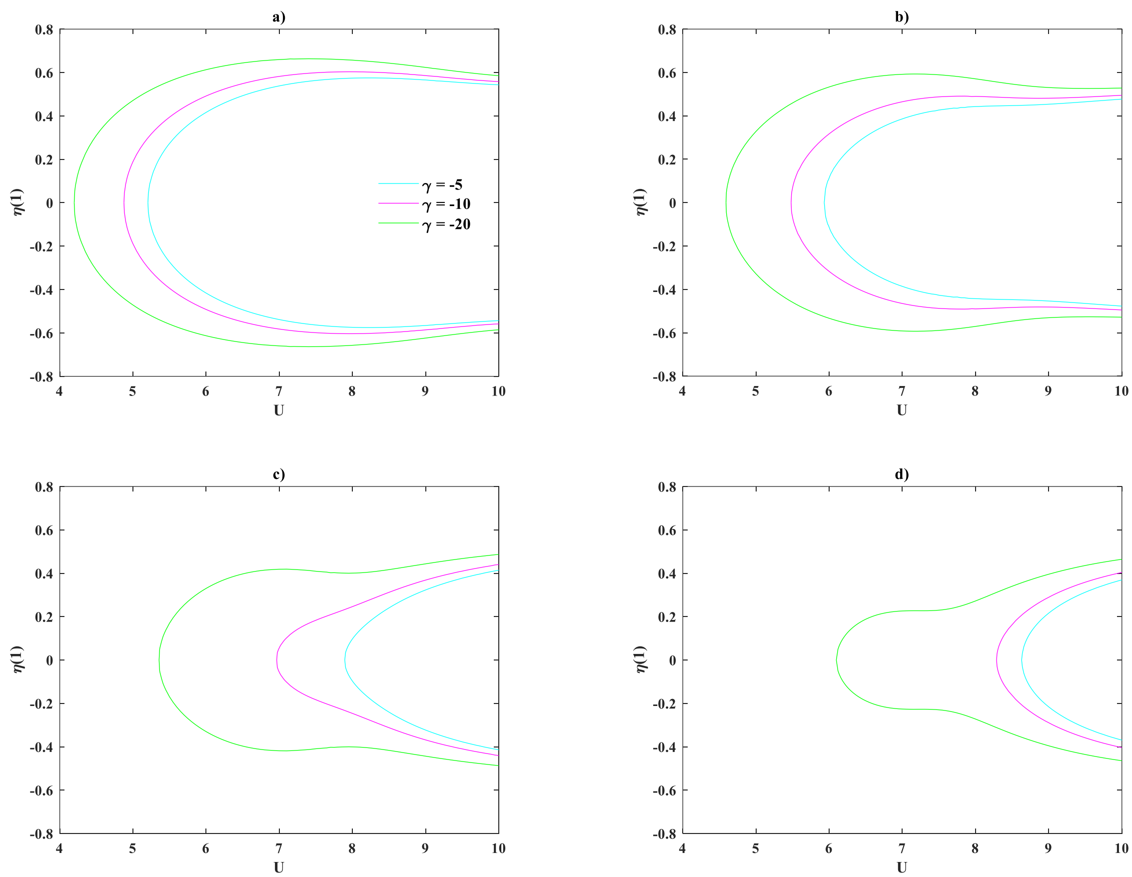

Figure 15: The tip transverse displacement of pipe in the post-flutter region corresponding to Figure 14; a) $\beta = 0.17$, b) $\beta = 0.25$, c) $\beta = 0.37$, d) $\beta = 0.45$.

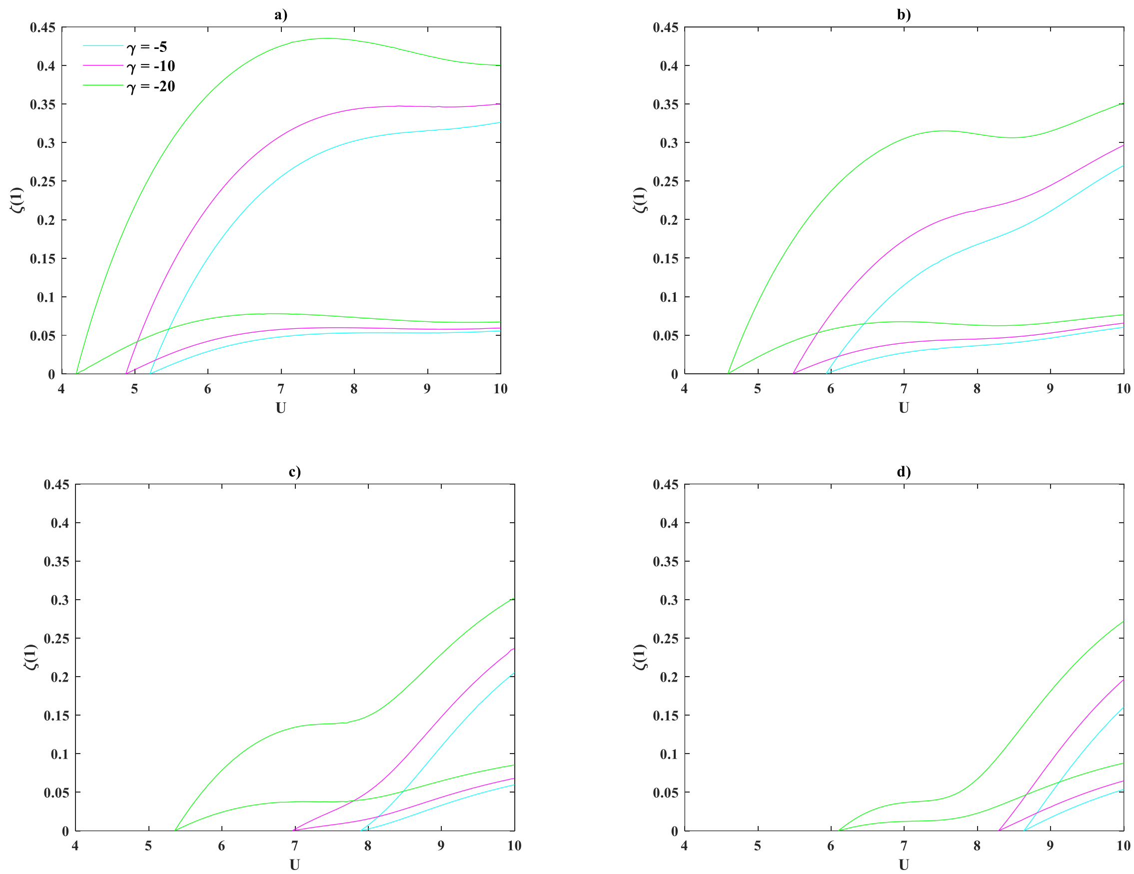

Figure 16: The tip axial displacement of pipe in the post-flutter region corresponding to Figure 14; a) $\beta = 0.17$, b) $\beta = 0.25$, c) $\beta = 0.37$, d) $\beta = 0.45$.

The general behavior of system with $\gamma = -30$ when $\beta = 0.17, 0.25, 0.37,$ and 0.45 is demonstrated in Figures 17-19 for the tip rotation angle, tip axial, and transverse displacements, respectively. For the system with $\gamma = -30$, the unstable and stable critical flow velocities associated with subcritical buckling occur at $U_{sub}^{low} = 3.0726$ and U_{sub}^{up} =4.0618, respectively. On the other hand, the critical flow velocities related to the flutter instability for values $\beta = 0.17, 0.25, 0.37,$ and 0.45 are $U^f = 3.4732, 3.690, 4.0836,$ and 4.3853, respectively. Comparing U_{sub}^{up} and U^f shows that for $\beta = 0.17$ and 0.25, U^f is smaller than U_{sub}^{up}. This means that for $U_{sub}^{low} < U < U^f$, the system exhibits three stable configurations including two symmetric stable positions resulting from subcritical buckling, in addition to its undeformed state. for $U^f < U < U_{sub}^{up}$, the system may undergo either post-buckling or post-flutter (see Figures 17-19 a-b). Since $U^f > U_{sub}^{up}$ for $\beta = 0.37$ and 0.45, a similar scenario to that described for the system with $\beta = 0.17$ and $\gamma = -20$ takes place for these cases. The described scenario for the system with $\gamma = -30$ when $\beta = 0.17$ or 0.25 can take place for $\beta = 0.37$ and 0.45 when the gravity parameter becomes sufficiently small in which $U^f < U_{sub}^{up}$ (see Figure 7).

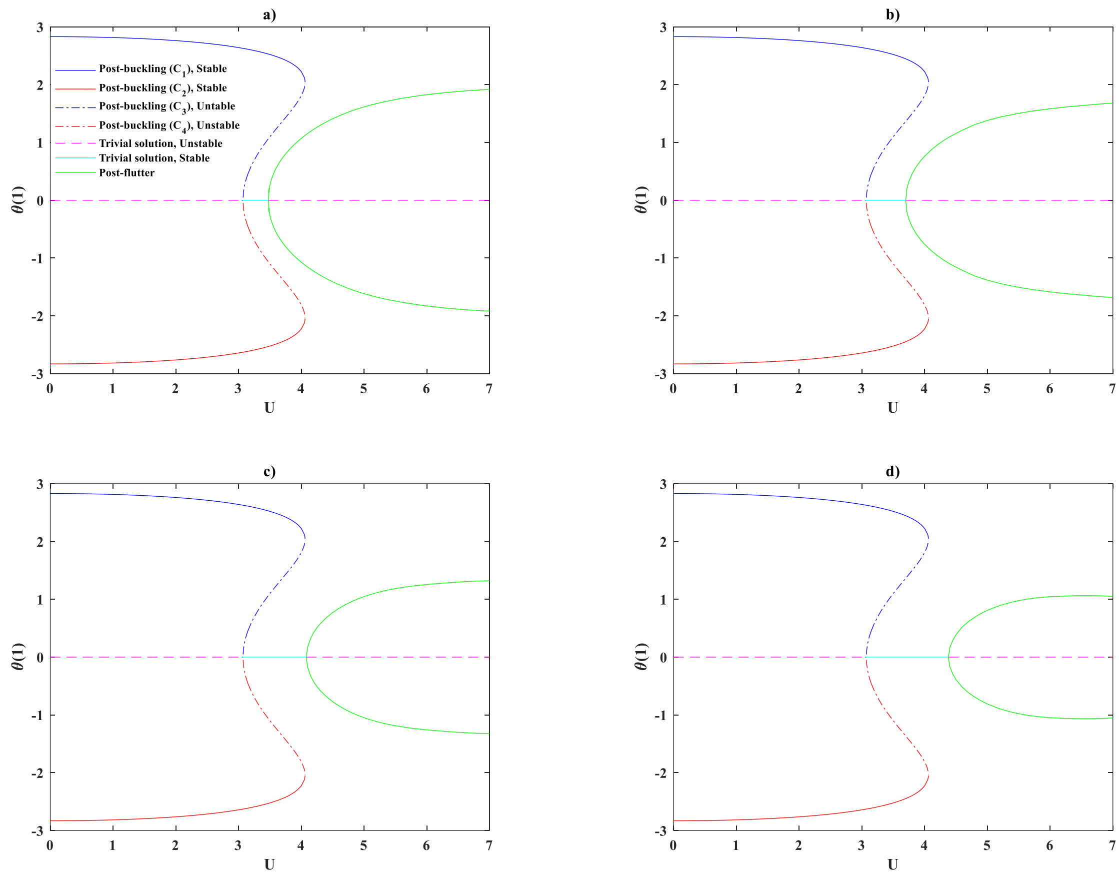

Figure 17: The tip rotation angle of pipe when $\gamma = -30$; a) $\beta = 0.17$, b) $\beta = 0.25$, c) $\beta = 0.37$, d) $\beta = 0.45$.

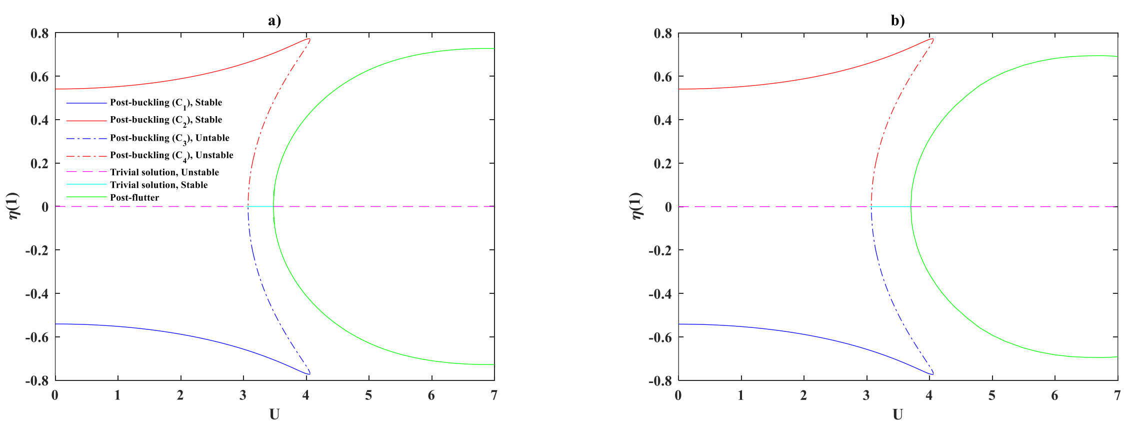

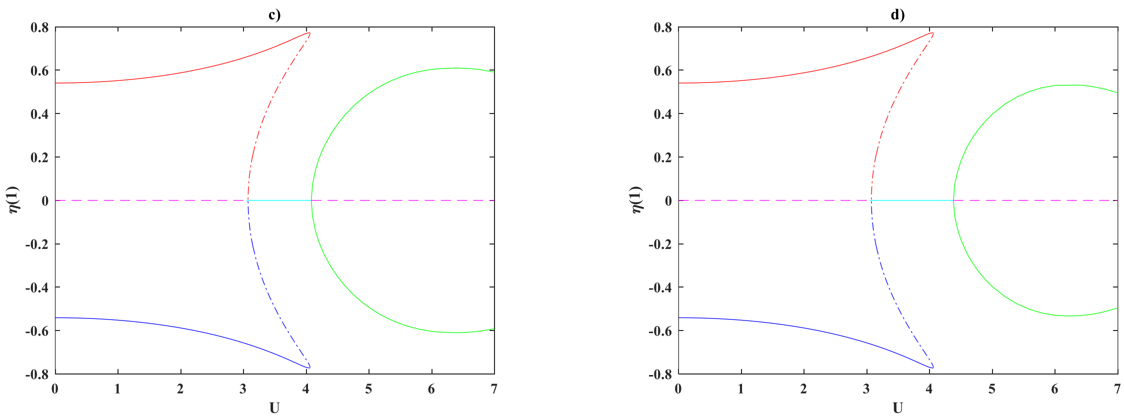

Figure 18: The tip transverse displacement of pipe of pipe corresponding to Figure 17; a) $\beta = 0.17$, b) $\beta = 0.25$, c) $\beta = 0.37$, d) $\beta = 0.45$.

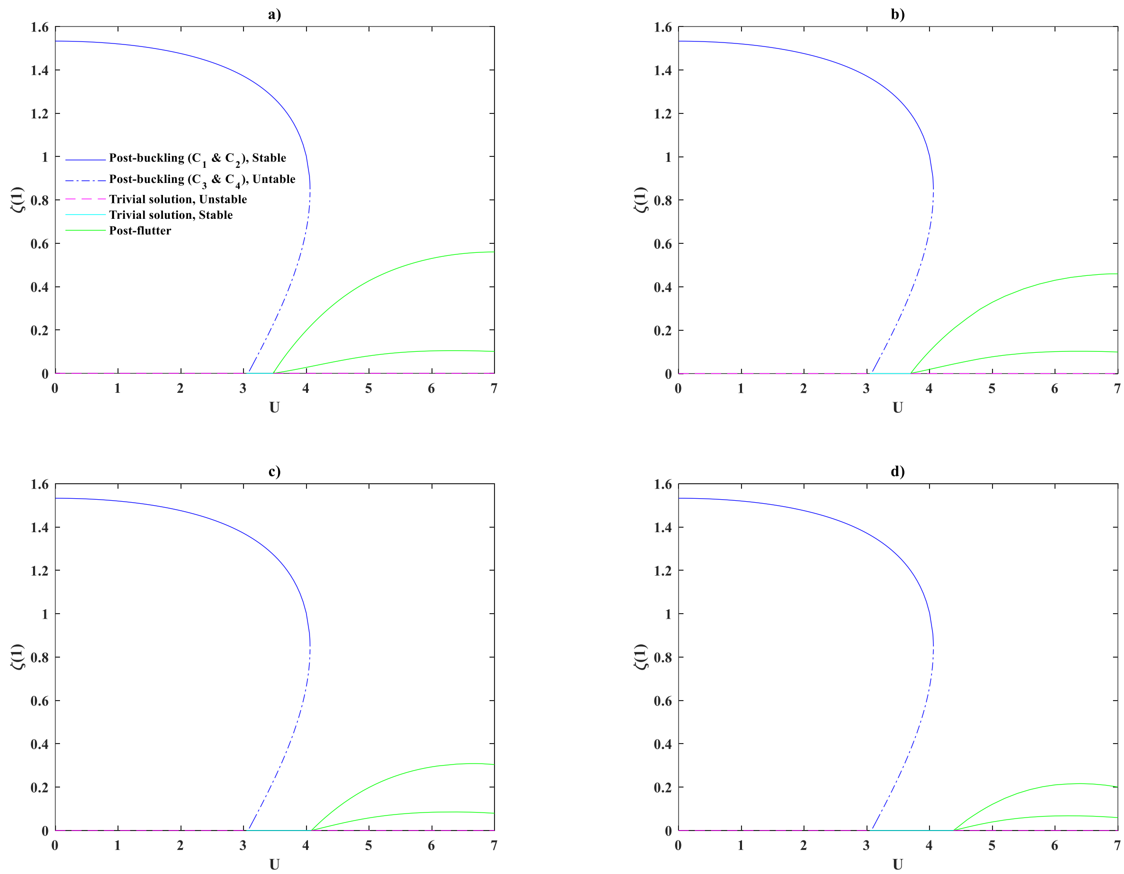

Figure 19: The tip axial displacement of pipe of pipe corresponding to Figure 17; a) $\beta = 0.17$, b) $\beta = 0.25$, c) $\beta = 0.37$, d) $\beta = 0.45$.

The general deformed shapes of system with $\gamma = -30$ and $\beta = 0.17$ for $U = 3, 3.25, 4$, and 4.25 are exhibited in Figure 20. The plotted results indicate that the system has two symmetric stable positions when $U = 3$, but it finds three stable positions when $U = 3.25$. Additionally, the system may undergo post-buckling or post-flutter when $U = 4$; however, it only undergoes post-flutter when $U = 4.25$. The dynamic responses of system for $U = 3.25$ and 4 under different initial conditions with positive values are plotted in Figure 21. The depicted results in Figure 21a corresponding to Figure 20b indicate that the system settles down at both the post-buckled position and the undeformed configuration, depending on the initial conditions. Besides, the results plotted in Figure 21b, which correspond to Figure 20c, illustrate that both post-buckling or post-flutter scenarios can occur for the system, depending on the initial conditions. However, both the plots in the figure show that the initial conditions do not affect the amplitude of post-buckled position and also the amplitude and frequency of post-flutter response. The responses of system with $\beta = 0.17$ and 0.45 when $U = 4.25$ are also shown in Figure 22. In the case of $\beta = 0.17$ corresponding to Figure 20c, the only response of system is post-flutter and in the case of $\beta = 0.45$ (see Figure 17a) the only response of system is its undeformed configuration. The plots in Figure 22 demonstrate that the final steady-state response is independent of the initial conditions for both cases.

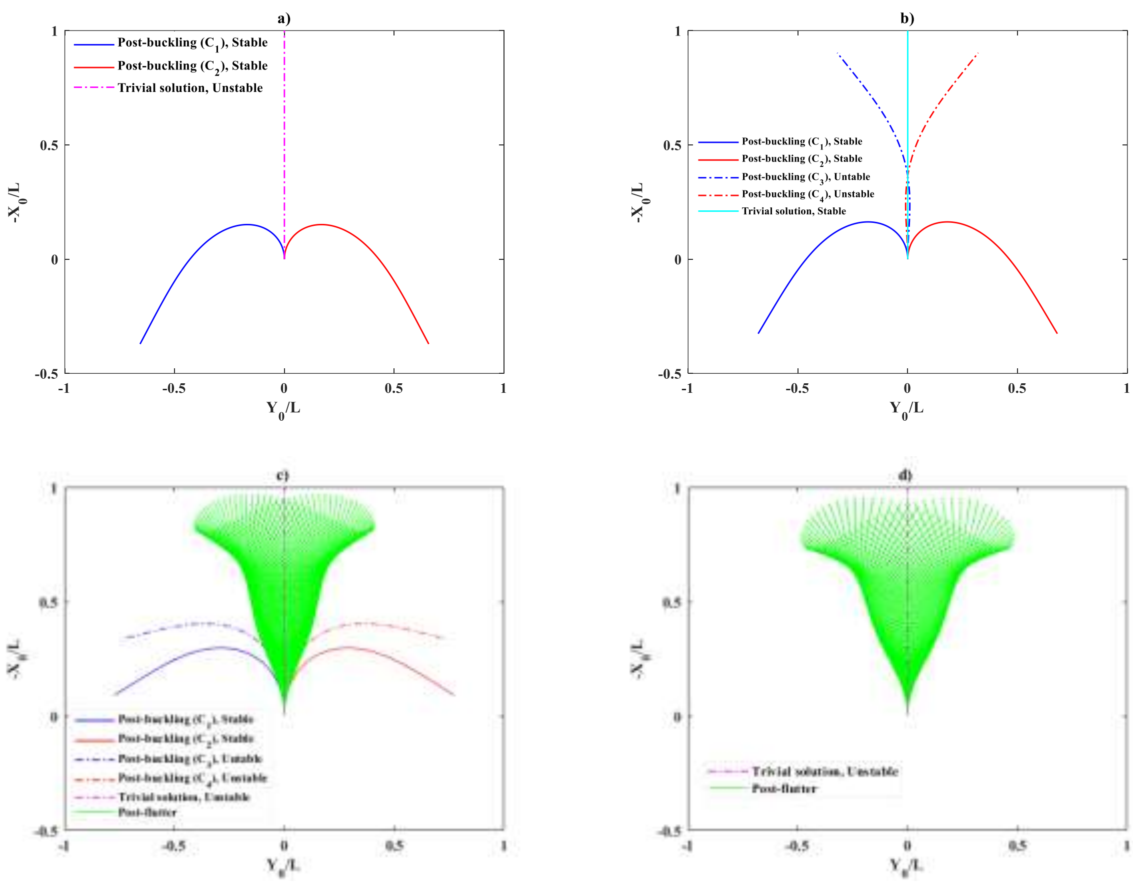

Figure 20: Shapes of the pipe when $\beta = 0.17$, $\gamma = -30$; a) $U = 3$, b) $U = 3.25$, c) $U = 4$, d) $U = 4.25$.

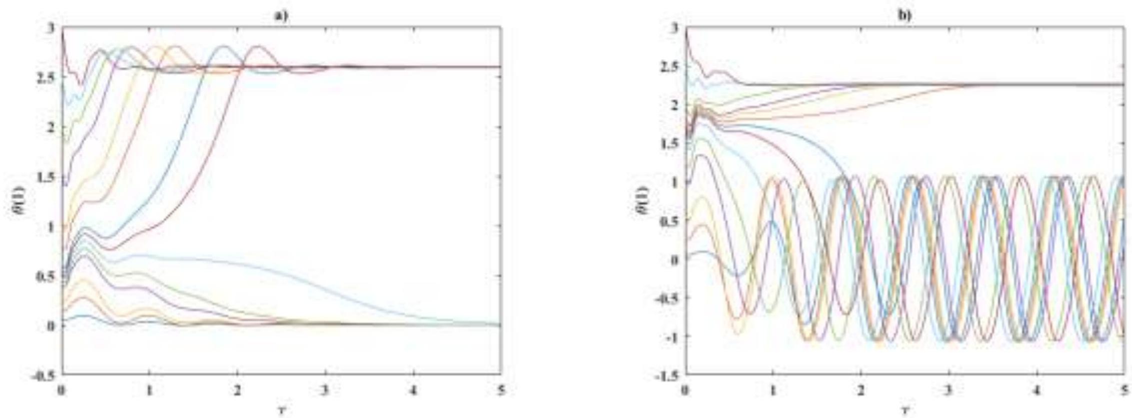

Figure 21: Time trace for the tip rotation of pipe under different initial conditions when $\beta = 0.17$, $\gamma = -30$; a) $U = 3.25$, b) $U = 4$.

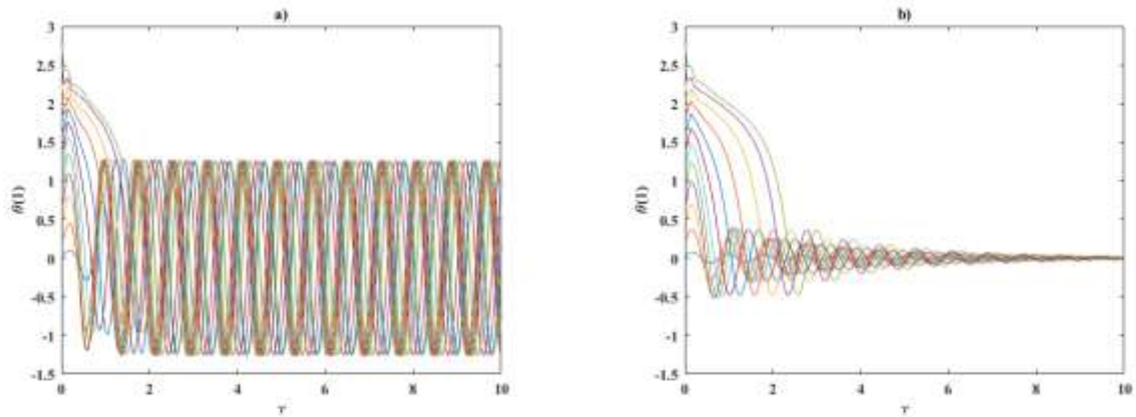

Figure 22: Time trace for the tip rotation of pipe under different initial conditions when $\gamma = -30$, and $U = 4.25$; a) $\beta = 0.17$, b) $\beta = 0.45$.

Eventually, it is intriguing to compare the results obtained from the geometrically exact nonlinear model with those derived from an approximate nonlinear model. For this comparative study, the third-order nonlinear model developed by Semler et al. [28], which is commonly used to investigate the nonlinear behavior of cantilevered pipes conveying fluid [3], is chosen. Since the model proposed by Semler et al. [28] is in terms of the transverse displacement, the comparative study focuses solely on the tip transverse displacement, similar to the approach taken by Farokhi et al. [44]. Figure 23 shows the results of this study, which are based on both the geometrically exact nonlinear model and the third-order nonlinear model for the system with $\beta = 0.17$ when $\gamma = -5$ and $\gamma = -10$. As observed, the results of the third-order nonlinear model align closely with those reported from the geometrically exact model when the amplitude of post-flutter or post-buckling is small. However, as the amplitude increases, the approximate nonlinear model tends to overestimate the tip transverse displacement. It is important to note that a similar outcome regarding the post-flutter behavior of hanging cantilevered pipes conveying fluid was reported by Farokhi et al. [44]. Furthermore, the plotted results indicate that the approximate nonlinear model is unable to accurately predict the static configuration of system across a wide range of flow velocities at which post-buckling occurs.

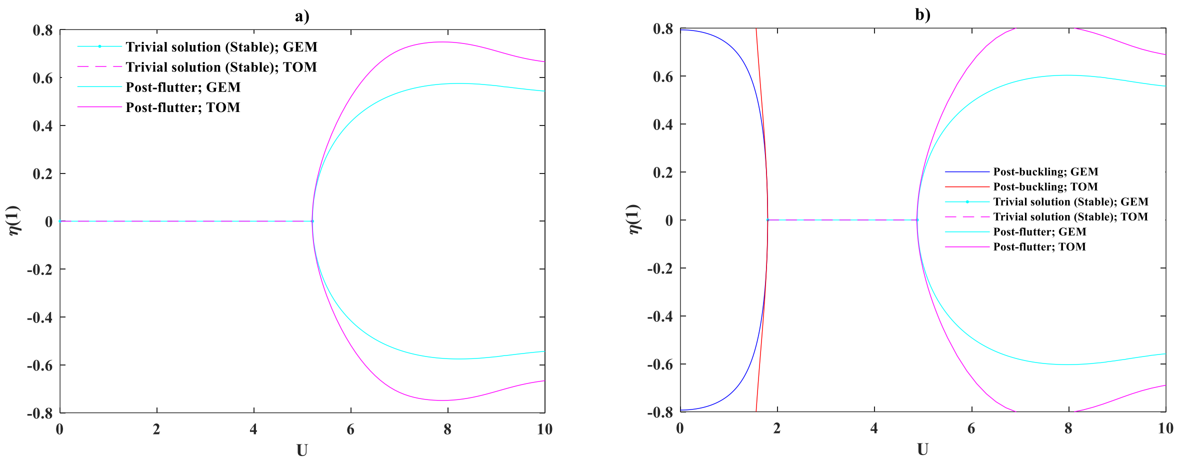

Figure 23: Comparison study between the geometrically exact model (GEM) and the third-order model (TOM) for $\beta = 0.17$; a) $\gamma = -5$ b) $\gamma = -10$.

5. Conclusion

In the current study, the geometrically exact static responses and their stability characteristics for a standing cantilevered pipe conveying fluid are examined when the gravity parameter falls within the range of $-100 \leq \gamma \leq 0$. The geometrically exact dynamic behavior, along with the generic behavior of system is also examined for $-30 \leq \gamma$, different values of the mass ratio $\beta = 0.17, 0.25, 37,$ and 0.45 when the flow velocity falls within the range of $0 \leq U \leq 10$. Additionally, the geometrically exact quaternion-based model utilized for the dynamic analysis is verified by comparing its results with those reported in Ref. [54] based on the geometrically exact rotation-based model.

The generic behavior of standing cantilevered pipe conveying fluid is significantly influenced by the gravity parameter, in contrast to the hanging one. It is due to the fact that a standing pipe with zero flow velocity may lose its stability and buckle under its own weight, potentially experiencing extremely large amplitudes. Therefore, its undeformed configuration may not be stable, in contrast to the hanging one. The standing cantilevered pipe conveying fluid undergoes supercritical and subcritical bucklings when $-14 \leq \gamma < -7.83$ and $\gamma < -14$, respectively. As well, the unstable critical flow velocity associated with the subcritical buckling becomes zero at $\gamma = -55.9$ and this critical flow velocity disappears for $\gamma > -55.9$. In the case of supercritical buckling, the amplitudes of stable post-buckled branches become zero as the flow velocity increases beyond a critical threshold. In contrast, the amplitudes of these stable branches do not reach zero in the case of subcritical buckling. Furthermore, within the subcritical buckling domain, the impact of increasing flow velocity on the system's deformation diminishes as the gravity parameter is lessened.

The system undergoes flutter instability due to a supercritical Hopf bifurcation, where the mass ratio, along with the gravity parameter plays a significant role in the critical flow velocity at which the flutter occurs. Additionally, these factors affect the motion characteristics of self-excited periodic oscillations in the post-flutter region (see Figure 14). The stability of undeformed configuration prior to flutter is dependent on the gravity parameter. In the case of $\gamma \geq -7.83$, the undeformed configuration remains stable before flutter occurs. In the supercritical or subcritical buckling domain, the system is initially unstable. It becomes stable at the supercritical flow velocity or the low subcritical flow velocity, but it subsequently loses stability again due to flutter. In light of the aforementioned supercritical/subcritical buckling and supercritical Hopf bifurcation, four distinct scenarios arise as the flow velocity increases. In the first scenario, the undeformed configuration of system is stable but becomes unstable due to a flutter instability (see Figure 8a), similar to the hanging one. In the second scenario, the undeformed configuration of system is unstable; however, it becomes stable through a supercritical buckling and remains stable until it loses stability due to flutter (see Figure 8b). In the third scenario, the system experiences subcritical buckling, resulting in a stable undeformed configuration at a lower subcritical flow velocity. However, it subsequently loses stability through a flutter, as illustrated in Figures 8c and 17c-d. A primary difference between this scenario and the previous one is that the undeformed configuration and the symmetric stable positions, resulting from subcritical buckling, represent the stable states of system when the flow velocity is between the lower and upper subcritical flow velocities. The fourth scenario is akin to the third, but it features a significant distinction. In this scenario, the critical flow velocity at which flutter instability occurs falls between the lower and upper subcritical flow velocities (see Figures 17a-b). In other words, the system experiences post-buckling or post-flutter behavior at certain flow velocities. Dynamic analyses that emphasize the role of initial conditions reveal that varying responses can be predicted for a specific case when suitable initial conditions are applied.

Appendix A

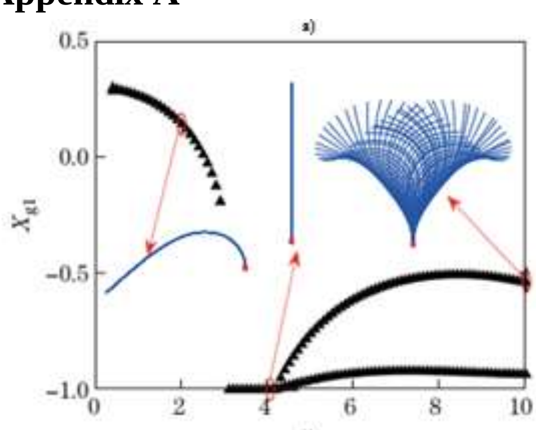

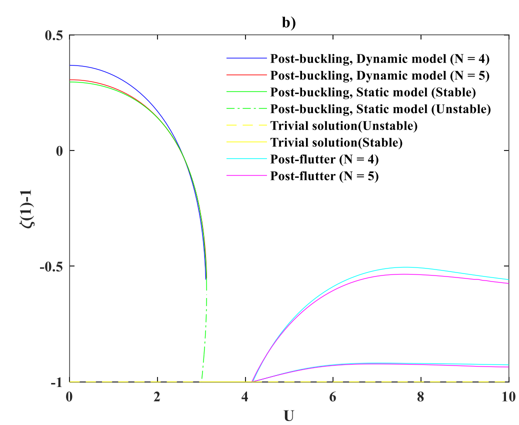

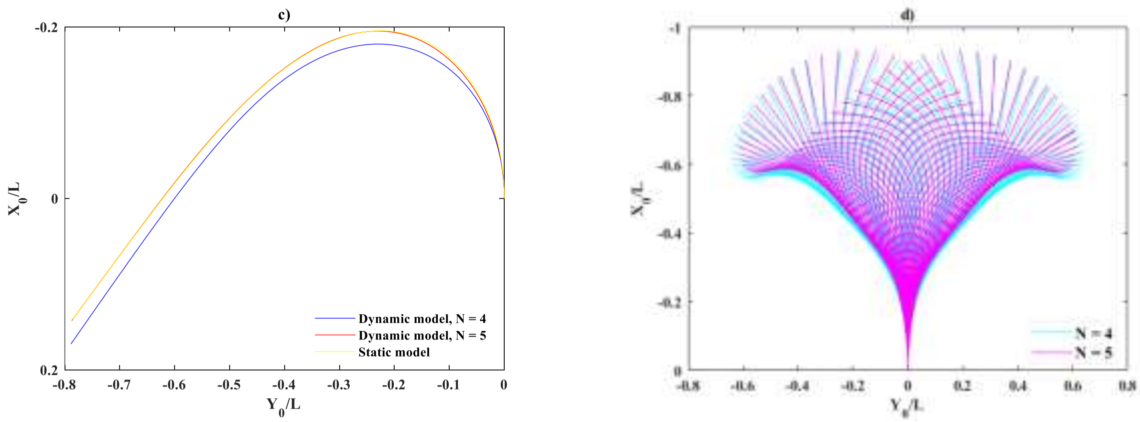

Figure A1: Comparison studies for the tip axial displacements and shapes of pipe when $\beta = 0.142$, $\gamma = -18.9$, and $\alpha = 0.005$ a) Chen et al. [54] via the geometrically exact rotation-based model with $N = 4$, b, c, and d) present study using the geometrically exact quaternion-based model with $N = 4$ & 5.

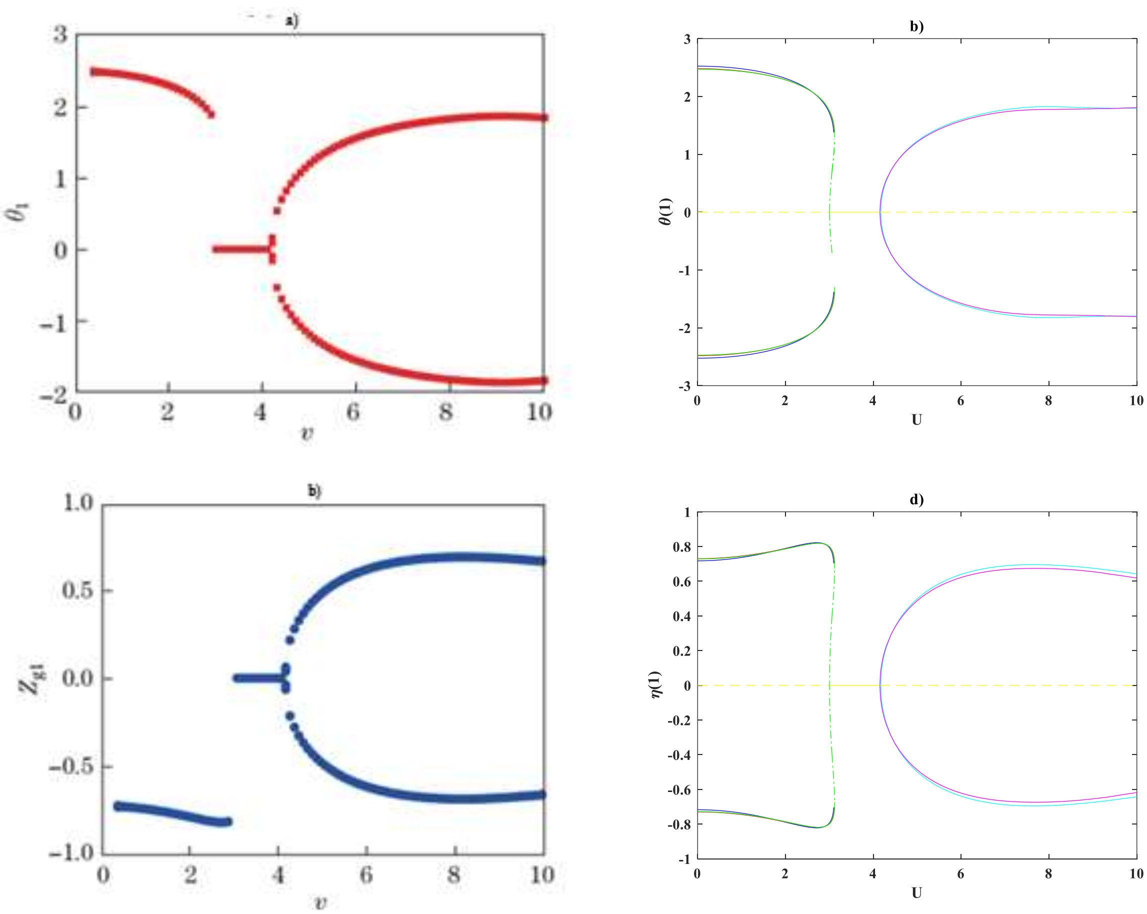

Figure A2: Comparison studies for the tip rotations and tip transverse displacements of pipe corresponding to Figure A1a-b; a & c) Chen et al. [54], b & d) present study.

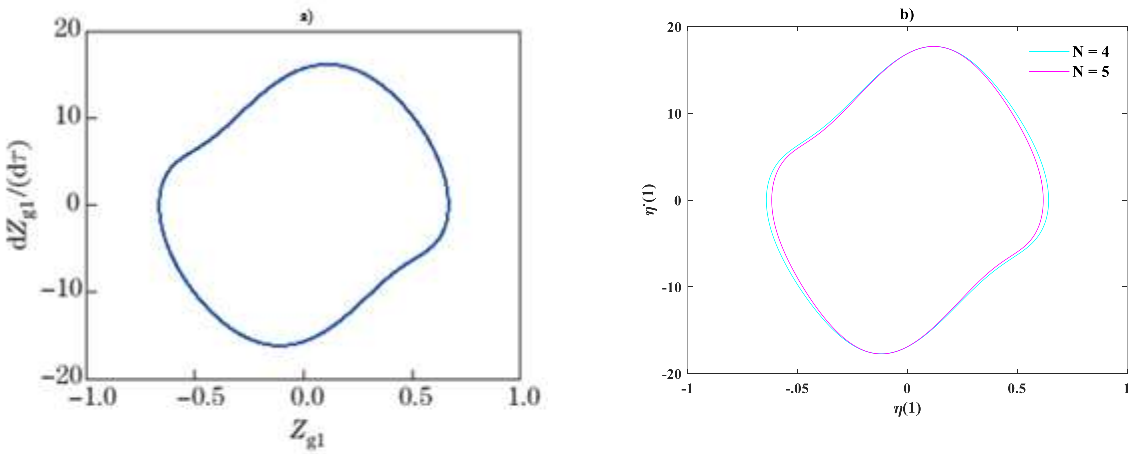

Figure A3: Comparison studies for the phase plane of pipe corresponding to Figure A1a & d; a) Chen et al. [54], b) present study.

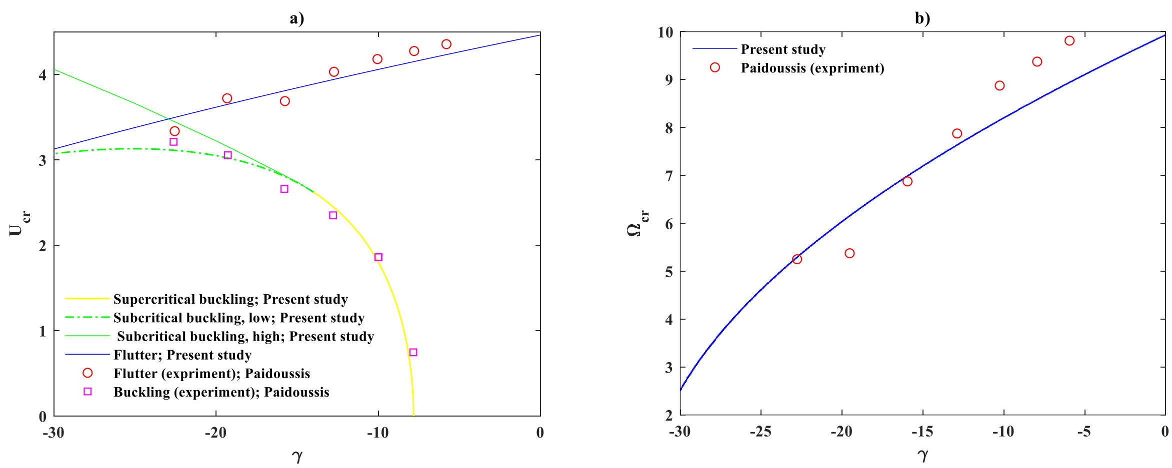

Figure A4: Comparison studies for the critical flow velocities and corresponding natural frequencies between the present model and those reported by Paidoussis [25] based on the experimental measurements for the system with $\beta = 1.1 \times 10^{-3}$.

References

[1] R. A. Ibrahim, "Overview of mechanics of pipes conveying fluids—Part I: Fundamental studies," *Journal of Pressure Vessel Technology, Transactions of the ASME,* vol. 132, no. 3, pp. 0340011 - 03400132, 2010.

[2] R. A. Ibrahim, "Mechanics of pipes conveying fluids—part II: applications and fluidelastic problems," *Journal of Pressure Vessel Technology, Transactions of the ASME*, vol. 133, no. 2, p. 024001, 2011.

[3] M. P. Païdoussis, *Fluid-structure interactions: slender structures and axial flow*, Second ed. Elsevier, 2014.

[4] M. P. Païdoussis, "Pipes conveying fluid: a fertile dynamics problem," *Journal of Fluids and Structures*, vol. 114, p. 103664, 2022.

[5] H. Ding and J. C. Ji, "Vibration control of fluid-conveying pipes: a state-of-the-art review," *Applied Mathematics and Mechanics*, vol. 44, no. 9, pp. 1423-1456, 2023.

[6] Q. Jin and Y. Ren, "Review on mechanics of fluid-conveying nanotubes," *International Journal of Engineering Science,* vol. 195, p. 104007, 2024.
[7] M. P. Paidoussis, "The canonical problem of the fluid-conveying pipe and radiation of the knowledge gained to other dynamics problems across applied mechanics," *Journal of Sound and Vibration,* vol. 310, no. 3, pp. 462-492, 2008.
[8] P. J. Holmes, "Pipes supported at both ends cannot flutter," *Journal of Applied Mechanics,* vol. 45, no. 3, pp. 619–622, 1978.
[9] M. Yoshizawa, H. Nao, E. Hasegawa, and Y. Tsujioka, "Buckling and postbuckling behavior of a flexible pipe conveying fluid," *Bulletin of JSME,* vol. 28, no. 240, pp. 1218-1225, 1985.
[10] M. Nikolić and M. Rajković, "Bifurcations in nonlinear models of fluid-conveying pipes supported at both ends," *Journal of Fluids and Structures,* vol. 22, no. 2, pp. 173-195, 2006.
[11] Y. Modarres-Sadeghi and M. P. Païdoussis, "Nonlinear dynamics of extensible fluid-conveying pipes, supported at both ends," *Journal of Fluids and Structures,* vol. 25, no. 3, pp. 535-543, 2009.
[12] Y.-L. Zhang and L.-Q. Chen, "External and internal resonances of the pipe conveying fluid in the supercritical regime," *Journal of Sound and Vibration,* vol. 332, no. 9, pp. 2318-2337, 2013.
[13] F. Liang, Y. Chen, J.-J. Gong, and Y. Qian, "Vibration self-suppression of spinning fluid-conveying pipes composed of periodic composites," *International Journal of Mechanical Sciences,* vol. 220, p. 107150, 2022.
[14] J.-R. Yuan and H. Ding, "Three-dimensional dynamic model of the curved pipe based on the absolute nodal coordinate formulation," *Mechanical Systems and Signal Processing,* vol. 194, p. 110275, 2023.
[15] B. Zhu, X. Zhang, and T. Zhao, "Nonlinear planar and non-planar vibrations of viscoelastic fluid-conveying pipes with external and internal resonances," *Journal of Sound and Vibration,* vol. 548, p. 117558, 2023.
[16] Y. Guo, J.-a. Li, B. Zhu, and Y. Li, "Nonlinear dynamical model of hyperelastic pipes conveying fluid with finite deformation: roles of hyperelasticity and nonlinearity," *Nonlinear Dynamics,* pp. 1-18, 2023.
[17] F. Liang, Y. Chen, H. Kou, and Y. Qian, "Hybrid Bragg-locally resonant bandgap behaviors of a new class of motional two-dimensional meta-structure," *European Journal of Mechanics-A/Solids,* vol. 97, p. 104832, 2023.
[18] Y. Tang, G. Wang, T. Yang, and Q. Ding, "Nonlinear dynamics of three-directional functional graded pipes conveying fluid with the integration of piezoelectric attachment and nonlinear energy sink," *Nonlinear Dynamics,* vol. 111, no. 3, pp. 2415-2442, 2023.
[19] M.-Y. Hao, H. Ding, X.-Y. Mao, and L.-Q. Chen, "Multi-harmonic resonance of pipes conveying fluid with pulsating flow," *Journal of Sound and Vibration,* vol. 569, p. 117990, 2024.
[20] F.-J. Bourrières, "Sur un phénomène d'oscillation auto-entretenue en mécanique des fluides réels," *Publications Scientifiques Et Techniques Du Ministère de L'air* vol. 147, 1939.
[21] T. B. Benjamin, "Dynamics of a system of articulated pipes conveying fluid-I. Theory," *Proceedings of the Royal Society of London. Series A. Mathematical and Physical Sciences,* vol. 261, no. 1307, pp. 457-486, 1961.

[22] T. B. Benjamin, "Dynamics of a system of articulated pipes conveying fluid. II. Experiments," *Proceedings of the Royal Society A: Mathematical, Physical and Engineering Sciences,* pp. 487-499, 1961.

[23] M. P. Païdoussis and R. W. Gregory, "Unstable oscillation of tubular cantilevers conveying fluid. I. theory," *Proceedings of the Royal Society of London,* vol. 293, no. 1435, pp. 512-527, 1966.

[24] R. W. Gregory and M. P. Paidoussis, "Unstable oscillation of tubular cantilevers conveying fluid II. Experiments," *Proceedings of the Royal Society of London. Series A. Mathematical and Physical Sciences,* vol. 293, no. 1435, pp. 528-542, 1966.

[25] M. P. Paidoussis, "Dynamics of tubular cantilevers conveying fluid," *Journal of Mechanical Engineering Science,* vol. 12, no. 2, pp. 85-103, 1970.

[26] A. K. Bajaj, P. R. t. Sethna, and T. S. Lundgren, "Hopf bifurcation phenomena in tubes carrying a fluid," *SIAM Journal on Applied Mathematics,* vol. 39, no. 2, pp. 213-230, 1980.

[27] A. K. Bajaj and P. R. Sethna, "Flow induced bifurcations to three-dimensional oscillatory motions in continuous tubes," *SIAM Journal on Applied Mathematics,* vol. 44, no. 2, pp. 270-286, 1984.

[28] C. Semler, G. X. Li, and M. Paıdoussis, "The non-linear equations of motion of pipes conveying fluid," *Journal of Sound and Vibration,* vol. 169, no. 5, pp. 577-599, 1994.

[29] M. Wadham-Gagnon, M. P. Paı, and C. Semler, "Dynamics of cantilevered pipes conveying fluid. Part 1: Nonlinear equations of three-dimensional motion," *Journal of fluids and structures,* vol. 23, no. 4, pp. 545-567, 2007.

[30] Y. Modarres-Sadeghi, M. P. Païdoussis, and C. Semler, "Three-dimensional oscillations of a cantilever pipe conveying fluid," *International Journal of Non-Linear Mechanics,* vol. 43, no. 1, pp. 18-25, 2008.

[31] M. H. Ghayesh, M. P. Païdoussis, and Y. Modarres-Sadeghi, "Three-dimensional dynamics of a fluid-conveying cantilevered pipe fitted with an additional spring-support and an end-mass," *Journal of Sound and Vibration,* vol. 330, no. 12, pp. 2869-2899, 2011.

[32] G. H. Chang and Y. Modarres-Sadeghi, "Flow-induced oscillations of a cantilevered pipe conveying fluid with base excitation," *Journal of Sound and Vibration,* vol. 333, no. 18, pp. 4265-4280, 2014.

[33] A. M. Dehrouyeh-Semnani, H. Zafari-Koloukhi, E. Dehdashti, and M. Nikkhah-Bahrami, "A parametric study on nonlinear flow-induced dynamics of a fluid-conveying cantilevered pipe in post-flutter region from macro to micro scale," *International Journal of Non-Linear Mechanics,* vol. 85, pp. 207-225, 2016.

[34] Y. Wang, L. Wang, Q. Ni, H. Dai, H. Yan, and Y. Luo, "Non-planar responses of cantilevered pipes conveying fluid with intermediate motion constraints," *Nonlinear Dynamics,* vol. 93, pp. 505-524, 2018.

[35] M. Kheiri, "Nonlinear dynamics of imperfectly-supported pipes conveying fluid," *Journal of Fluids and Structures,* vol. 93, p. 102850, 2020.

[36] K. Yamashita, N. Nishiyama, K. Katsura, and H. Yabuno, "Hopf-Hopf interactions in a spring-supported pipe conveying fluid," *Mechanical Systems and Signal Processing,* vol. 152, p. 107390, 2021.

[37] Y. Guo, B. Zhu, and Y. Li, "Flow-induced instability and bifurcation in cantilevered composite double-pipe systems," *Ocean Engineering,* vol. 258, p. 111825, 2022.

[38] K. Yamashita, K. Kitaura, N. Nishiyama, and H. Yabuno, "Non-planar motions due to nonlinear interactions between unstable oscillatory modes in a cantilevered pipe conveying fluid," *Mechanical Systems and Signal Processing,* vol. 178, p. 109183, 2022.
[39] M. Riazat and M. Kheiri, "Three-dimensional nonlinear dynamics of imperfectly supported pipes conveying fluid," *Journal of Fluids and Structures,* vol. 123, p. 104011, 2023.
[40] M. H. Ghayesh, M. P. Païdoussis, and M. Amabili, "Nonlinear dynamics of cantilevered extensible pipes conveying fluid," *Journal of Sound and Vibration,* vol. 332, no. 24, pp. 6405-6418, 2013.
[41] J. Rivero-Rodriguez and M. Pérez-Saborid, "Numerical investigation of the influence of gravity on flutter of cantilevered pipes conveying fluid," *Journal of Fluids and Structures,* vol. 55, pp. 106-121, 2015.
[42] S. Tang and B. Sweetman, "A geometrically-exact momentum-based nonlinear theory for pipes conveying fluid," *Journal of Fluids and Structures,* vol. 100, p. 103190, 2021.
[43] W. Chen, H. Dai, Q. Jia, and L. Wang, "Geometrically exact equation of motion for large-amplitude oscillation of cantilevered pipe conveying fluid," *Nonlinear Dynamics,* vol. 98, pp. 2097-2114, 2019.
[44] H. Farokhi, M. Tavallaeinejad, and M. P. Païdoussis, "Geometrically exact dynamics of cantilevered pipes conveying fluid," *Journal of Fluids and Structures,* vol. 106, p. 103364, 2021.
[45] W. Chen, H. Dai, and L. Wang, "Three-dimensional dynamical model for cantilevered pipes conveying fluid under large deformation," *Journal of Fluids and Structures,* vol. 105, p. 103329, 2021.
[46] W. Chen, K. Zhou, L. Wang, and Z. Yin, "Geometrically exact model and dynamics of cantilevered curved pipe conveying fluid," *Journal of Sound and Vibration,* vol. 534, p. 117074, 2022.
[47] R. Cao, Z. Guo, W. Chen, H. Dai, and L. Wang, "Nonlinear dynamics of a circular curved cantilevered pipe conveying pulsating fluid based on the geometrically exact model," *Applied Mathematics and Mechanics,* vol. 45, no. 2, pp. 261-276, 2024.
[48] W. Chen, L. Wang, and Z. Peng, "A magnetic control method for large-deformation vibration of cantilevered pipe conveying fluid," *Nonlinear Dynamics,* vol. 105, pp. 1459-1481, 2021.
[49] A. M. Dehrouyeh-Semnani, "Nonlinear geometrically exact dynamics of fluid-conveying cantilevered hard magnetic soft pipe with uniform and nonuniform magnetizations," *Mechanical Systems and Signal Processing,* vol. 188, p. 110016, 2023.
[50] A. M. Dehrouyeh-Semnani, "A quaternion-based mathematical model for geometrically exact dynamic analysis of cantilevered pipe conveying fluid," *Nonlinear Dynamics,* vol. 112, pp. 9845–9869, 2024.
[51] G. X. Li and M. P. Paidoussis, "Stability, double degeneracy and chaos in cantilevered pipes conveying fluid," *International Journal of Non-linear Mechanics,* vol. 29, no. 1, pp. 83-107, 1994.
[52] L. Wang and Q. Ni, "A note on the stability and chaotic motions of a restrained pipe conveying fluid," *Journal of sound and vibration,* vol. 296, no. 4-5, pp. 1079-1083, 2006.
[53] N. M. Bou-Rabee, L. A. Romero, and A. G. Salinger, "A multiparameter, numerical stability analysis of a standing cantilever conveying fluid," *SIAM journal on applied dynamical systems,* vol. 1, no. 2, pp. 190-214, 2002.

[54] W. Chen, Z. Hu, H. Dai, and L. Wang, "Extremely large-amplitude oscillation of soft pipes conveying fluid under gravity," *Applied Mathematics and Mechanics,* vol. 41, no. 9, pp. 1381-1400, 2020.
[55] H. Farokhi, Y. Xia, and A. Erturk, "Experimentally validated geometrically exact model for extreme nonlinear motions of cantilevers," *Nonlinear Dynamics,* vol. 107, no. 1, pp. 457-475, 2022.
[56] H. Farokhi, E. Kohtanen, and A. Erturk, "Extreme parametric resonance oscillations of a cantilever: An exact theory and experimental validation," *Mechanical Systems and Signal Processing,* vol. 196, p. 110342, 2023.
[57] B. D. Texier and S. Dorbolo, "Deformations of an elastic pipe submitted to gravity and internal fluid flow," *Journal of Fluids and Structures,* vol. 55, pp. 364-371, 2015.